POLITECNICO DI TORINO

master's Degree in Automotive engineering

master's Degree Thesis

Development and assessment of a kinematic model for an L7 electric vehicle

Supervisors

Prof. Daniela Anna Misul

PhD student Claudio Maino

Candidate

Francesco Giontella

Academic year 2019/2020

Summary

The object of this work is battery electric vehicles belonging to the L7 class. Starting from the experimental data obtained through road tests of an electric quadricycle, the thesis aims to build a model able to simulate the performance and energy consumption of the vehicle. The proposed model follows a direct kinematic approach, i.e. having as input a speed profile is able to calculate for each instant the corresponding angular speeds and loads applied to the electric motor. From the mechanical power, it sets to the electric machine, the model switches to the electric power needed to follow the cycle and finally obtains the trend of the battery state of charge. The model has been built using MATLAB and Simulink and all powertrain components have been dimensioned using information available on the tested vehicle or in literature for the L7 category. The model was finally validated by imposing as input the speed profile collected during the driving missions and the related measured and simulated SOC trend were compared. Finally, the results obtained from the simulations are used to define a cycle and test procedures for the assessment of energy efficiency suitable for this category.

A mio padre,
che ai miei occhi è sempre stato e sempre sarà un eroe
a mia sorella,
e alla dolcezza e testardaggine che l'accompagnano sempre
a mia mamma,
la donna piu forte che conosca
che ha sempre creduto in me e che sempre continuerà a spronarmi
a agli gli amici
con cui ho riso lungo questo viaggio
grazie.

Table of Contents

List of Tables

List of Figures

Chapter 1

Introduction

1.1 Motivation for this work

In the last decads, air pollution due to vehicles with oil-derived fuels is increasing, especially carbon dioxide, one of the major causes of global warming. The report of the European Environment Agency (EEA) of 2017 states that in Europe the 22% of the GHG is produced by land transport of which in turn 60% is due to passenger transport. Moreover, these percentages are growing dramatically, with transport sector emissions rising by 2.2% compared to the previous year.
In response to this increase in air pollution, the European Commission issued a mandatory carbon dioxide reduction program initially for LDV [1, p. 2009] and then also for HDV [2, p. 2019].These tight limits on the CO_2 accompanied by credits for low and zero-emission vehicles have led automakers to introduce electric vehicles into their fleet.
Electric vehicles can be hybrid or BEV: the former combine at least two traction systems (one BEV and the other based on an ICE or fuel cell) and the latter are electric vehicles whose only on-board energy source is the battery.

In this thesis we will deal with BEVs whose main advantage compared to ICE vehicles are:

1. BEVs that are powered by an electric motor offers a complete environmental solution at the local level, instead, ICE generates pollutant gas emissions such as CO, NOX, PM and unburned HC and higher noise.

2. Higher tank-to-wheel efficiency of BEVs that is about 80% than an ICE vehicles that is about 30% − 40%. However, to have a correct comparison between the two types of propulsion it is necessary to use well-to-wheel efficiency considering the whole cycle of production and energy usage. Therefore the

improvement in energy efficiency of BEVs is strictly related to the method used to produce the electricity.

3. In BEVs, the use of an electric motor enables regenerative braking, i.e. during braking the vehicle it is able to recover part of the kinetic energy of the vehicle that it uses to recharge the batteries.

The main drawbacks of this technology are:

1. limited range in general $100 - 200km$ in real driving condition mainly due to the lower specific energy of batteries that is about two order om magnitude less than liquid fuel. Also, battery recharging is very time consuming typically 8-10h compared to filling a tank that only takes a few minutes, although it can be reduced by fast charging.

2. The higher purchase price of the vehicle compared to an ICE-based equivalent, due to the high cost of the battery pack which is for lithium-ion battery packs of around $300/kWh$

3. Besides, the presence of the battery also affects the weight of the BEV, in fact they are typically heavier than about 200-300kg compared to a similar ICE based vehicle.

4. While for vehicles fuelled by oil-derived fuels there is an extensive infrastructure for the distribution of fuel, for electric vehicles the recharging columns are not yet sufficiently widespread.

From these considerations, results that BEVs are not suitable for extra-urban driving condition that are characterized by long-distance journeys at high speeds, which do tot allow good exploiting of the regenerative brake. On the other hand, the transition to BEV in urban mobility is much easier because it is characterized by lower autonomy and speed requirements of vehicles. In addition, the greater dynamism typical of urban driving allows for better use of the regenerative brake.

At present, European cities are even more congested due to the increase in urban population and the consequent demand and use of motor vehicles, and about 50% of co2 emitted in these centers is due to transport. The road-map adopted by the European Commission [3, p. 2011] promotes a gradual phase-out of "conventionally fuelled" vehicles from the urban environment by promoting a significant reduction in oil dependence, greenhouse gas emissions, and local air and noise pollution, which will have to be complemented by the development of adequate refueling/recharging infrastructure for new vehicles. It also encourages the use of public transport for collective mobility and regarding personal transport it states that the use of smaller, lighter and more specialized road passenger transport vehicles should be stimulated.

These features can be found in vehicles belonging to the category L defined by European Parliament [4, p. 2013] that includes: Mopeds, Motorcycles, Motor Tricycles, and Quadricycles. BEV belonging to this category are smaller and lighter than a car and require smaller and therefore more economical battery systems due to the less energy demand.
Despite the variety of vehicles included in this category and their growing popularity, the European Commission has defined much less detailed approval procedures for this category of vehicles than for LDV and HDV, especially for those powered by electric propulsion.

1.2 Objectives and structure of the work

Understanding the importance that L-category BEV vehicles are destined to assume in urban mobility, this work aims to analyze the energy consumption of an electric quadricycle (category L7). Starting from experimental data collected during road tests, a kinematic model representative of this vehicle is built and validated. Finally, through the analysis of the results obtained, an enegy efficiency test procedure is proposed for this category of vehicles.
The thesis is divided into five chapters: Chapter 2 explains the construction of the Simulink model in all its parts and assumptions; Chapter 3 identifies the necessary parameters for the model and tests it through simulations on homologous cycles; Chapter 4 uses the experimental data to make sensitivity analyses with the aim of identifying the definitive parameters of the model and validate it; Chapter 5 elaborates the results of the model with the aim to define a suitable test procedure for the evaluation of the energy consumption and maximum range of BEV's of category L7; Finally, there are the conclusions in which some criticalities and suggestions for improvement of the model are proposed.

Chapter 2

Vehicle model

This chapter describes the design of the kinematic model of an electric vehicle.The purpose of the model is to estimate the battery charge and therefore the energy consumed by the vehicle following a speed cycle. The model has been elaborated on Simulink and is composed of sub-models representing the elements of the powertrain and the on-board electric energy source: wheels, final drive, gearbox, electric machine, inverter and battery system. Whereas an accurate description of the vehicle dynamics is not necessary, but only of the power levels in the various sections of the drive-line, it has been chosen to use a direct model which has a reduced computational cost and gives the possibility to be run in real time.

2.1 Resistant Power

The first Simulink sub-model is shown in figure 2.1. The input block is the cycle speed profile, i.e. the vector containing the velocity values at which the vehicle moves for each instant of the driving mission. The outputs are the total resistant force and power, which must be contrasted in order to move the quadricycle. The resistant forces that the model takes into consideration are: Rolling resistance, Grade resistance, Aerodynamic resistance and Inertia resistance. Once these have been evaluated, the Resistant Power is obtained by a multiplication between total Resistant Force and speed. The meaning of these forces and the related formulation used in the Simulink model are analyzed below.

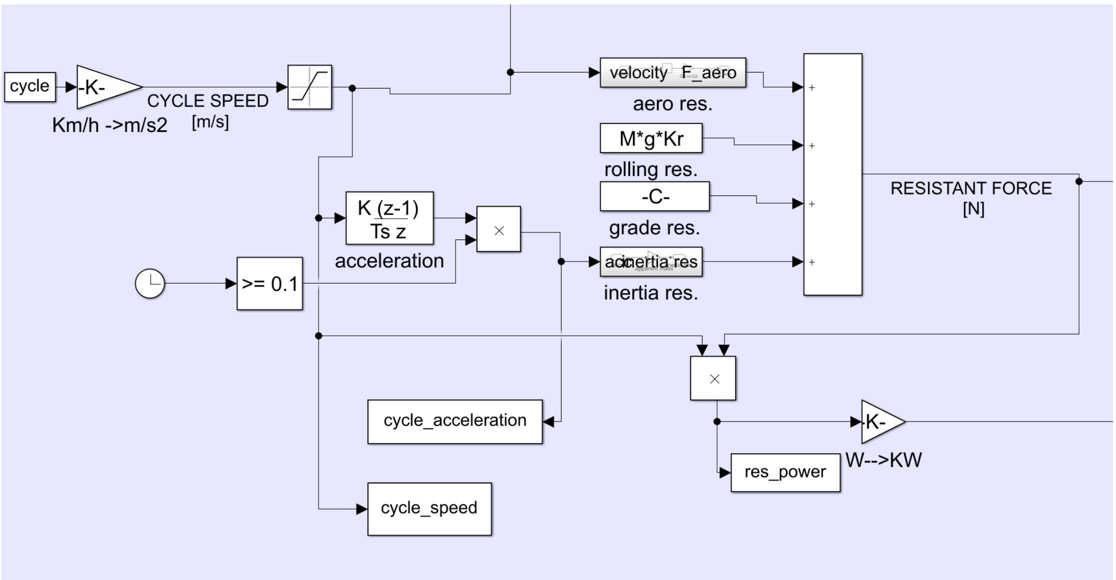

Figure 2.1: Simulink Resistant Power Sub-model

2.1.1 Resistant Forces

Rolling resistance

Rolling resistance is a force acting against the movement of a body that rolls on a surface.To understand its origin it is necessary to analyze the contact patch between the rolling body and the surface below. For example, the portion of the tyre entering the contact zone is deformed and when it leaves this region it recovers the deformation. To produce this deformation it is necessary to expend a certain amount of energy that is not completely recovered at the end of the contact, this is due to the internal damping of the material, in fact the rubber undergoes to hysteresis. The rolling resistance is mainly due to this energy dissipation. The rolling friction coefficient K_r modellization is very complex due to the dependence of the described phenomena on many factors such as the velocity, the tyre pressure and material, ecc. There are a lot of complex models that try to describe it using a polynomial function and experimental estimated coefficients (for instance the Pacejka "Magic formula"). A very simplified formulation of rolling resistance has been used in the model, which also ignores the dependence on speed. The assumption that the coefficient is independent of velocity is acceptable when considering that the vehicle in question is designed for urban driving and therefore subject to a small range of speed variation. Therefore the rolling resistance is computed as the rolling resistance coefficient K_r times the sum of forces normal to the plane N.

$$N = m \cdot g \cdot \cos(\alpha)$$

Where α showed in figure 2.2 represents the inclination of the road and $\cos(\alpha)$ is null on a flat road.

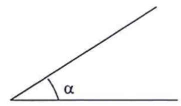

Figure 2.2: Slope road angle α definition.

$$F_r = m \cdot g \cdot K_r \cos(\alpha)$$

Grade resistance

In the case in which the road is not flat it is necessary to overcome also the component of the weight force tangential to the plane.

$$F_g = m \cdot g \cdot \mathrm{sen}(\alpha)$$

Aerodynamic resistance

Aerodynamic resistance is a force that counteract the relative motion of any object with respect to the surrounding fluid. It is not dependent on the mass of the object but only on its frontal area A_f and its shape C_x. It is also dependent on the square of the relative speed V and the density of the fluid ρ.

$$A_r = \frac{1}{2} \cdot \rho \cdot A_f \cdot C_x \cdot V^2$$

Inertia resistance

The inertia resistance is a force that act against the variation of velocity of an object. Concerning a car is due to both the mass of the vehicle that react to a longitudinal acceleration and to the rotating components of powertrain and wheels that reacts against angular acceleration.

$$A_i = M_{at} \cdot a \cdot V = m \cdot C_{at} \cdot a \cdot V$$

where M_{at} is the apparent translating mass of the vehicle; this parameters consider a vehicle that has the same overall kinetic energy of the real one and that moves as solid body in the longitudinal direction with the same speed. The apparent mass due to each rotating component is: the rotating inertia I_i times the square of its transmission ratio τ_i respect the wheels and divided by the square of wheel rolling radius r_d.

$$M_{at} = m + \sum \frac{I_i \cdot \tau_i^2}{r_d^2}$$

The inertial resistance is calculated from the acceleration obtained by speed derivation. As is possible to see in the model map in figure 2.1,for the first time step of the simulation the acceleration value is imposed to zero, because some velocity cycles starts with not null speed, this causes an error in the derivative, which results as an incoherent peak in the acceleration.

2.2 Transmission

This second sub-model is directly connected with the previous one, the inputs are the resistant force, resistant power and the cycle speed. The aim of this part of the Simulink code showed in figure 2.3 is to evaluate the torque T and the angular speed ω at the different stages of transmission. For this vehicle the stages considered are: wheels, final drive and gearbox.

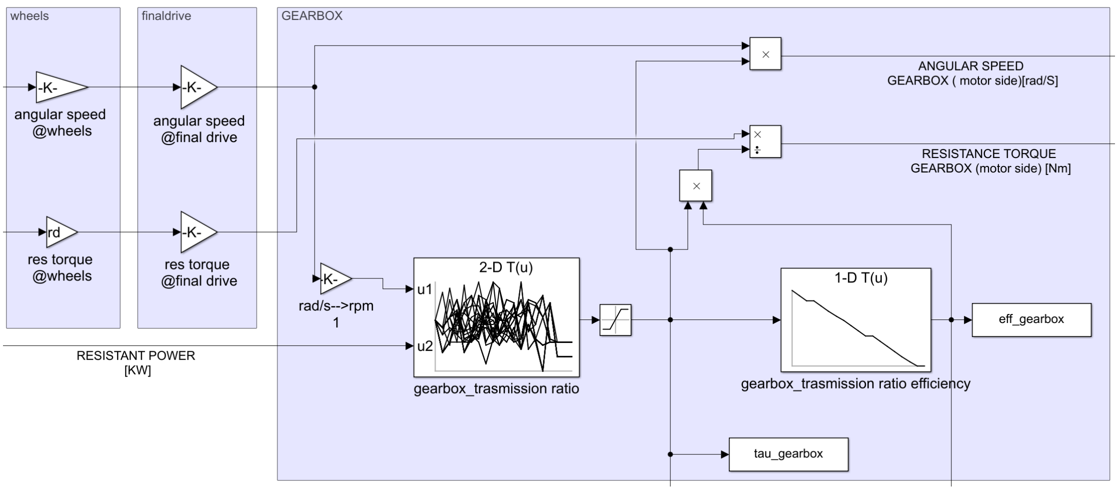

Figure 2.3: Simulink Transmission Sub-model

The vehicle speed is divided by the rolling radius r_d of the wheel obtaining the angular speed ω_w that is in turn multiplied by the transmission ratios of final drive τ_{fd} and gearbox τ_g obtaining the angular speed at final drive ω_{fd} and at gearbox ω_g (motor side).

$$\omega_w = \frac{V}{r_d} \qquad \omega_{fd} = \omega_w \cdot \tau_{fd} \qquad \omega_m = \omega_g = \omega_{fd} \cdot \tau_g$$

The resistant force is divided by the rolling radius obtaining the resistant torque at wheels T_w which is then divided by the final drive and gearbox transmission ratios and by the respective efficiencies η_{fd}, η_g.

$$T_w = \frac{F_r}{r_d} \qquad T_{fd} = \frac{T_w}{\tau_{fd} \cdot \eta_{fd}} \qquad T_g = \frac{T_{fd}}{\tau_g \cdot \eta_g}$$

Unlike final drive transmission ratio and efficiency that are are fixed values, the gearbox is a continuously variable transmission (CVT), therefore to modeling it are necessary a range of values of efficiency and transmission ratios .

2.2.1 Gearbox

Due to lacking of any direct information on the CVT gearbox, it been chosen to derive experimentally the transmission ratio values τ_g as a function of final drive angular speed ω_{fd} and resistant mechanical power P_r from the data recorded by the vehicle during the driving cycles. For each instant of the vehicle's driving missions the engine rpm n and vehicle speed are measured. from the vehicle speed it is possible to compute the resistant power and the angular speed at final drive ω_{fd}. Then the gearbox transmission ratio τ_g is computed as:

$$\tau_g = \frac{n \cdot \frac{2\pi}{60}}{\omega_{fd}} \quad function(P_r, \omega_{fd})$$

The gearbox transmission ratios are collected in a high resolution matrix $[100 \times 100]$ in which are classified in function of resistant power P_r and final drive angular speed ω_{fd}. The unknown elements of the matrix are compute using MATLAB interpolation function using the "Nearest" interpolation method. The interpolated high resolution matrix 3D plot and contour plot reported in figures 2.4,2.5 shows some peaks due to outliers values of $\tau_g > 7$.

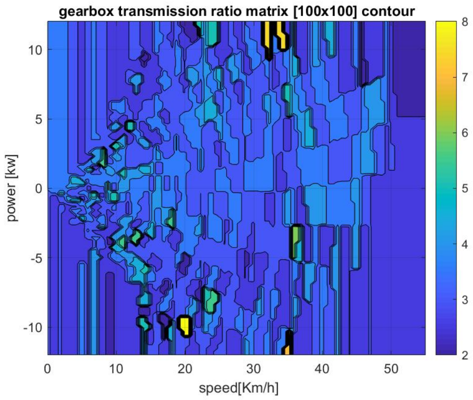

Figure 2.4: τ_g matrix [100x100] contour

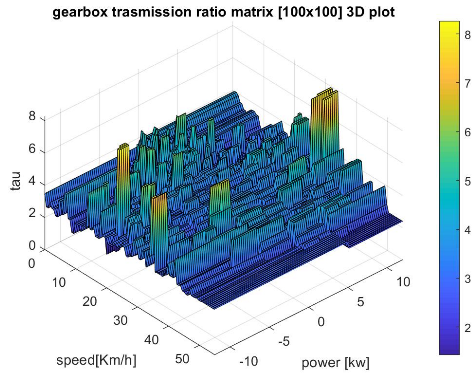

Figure 2.5: τ_g matrix [100x100] 3D plot

From the high resolution matrix by means of another interpolation, a smaller one [20x25] has been obtained and in doing so the importance of the outliers has also been limited. In fact, as can be seen in the figure 2.6, the peaks have been considerably reduced.

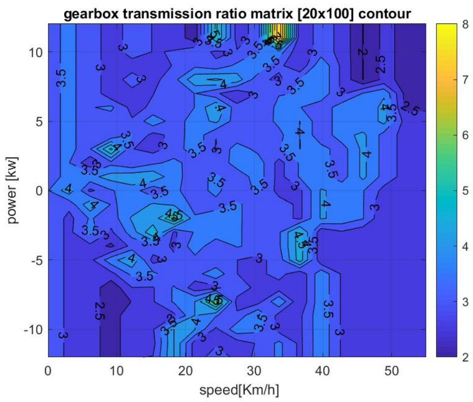

Figure 2.6: τ_g matrix [20x25] contour

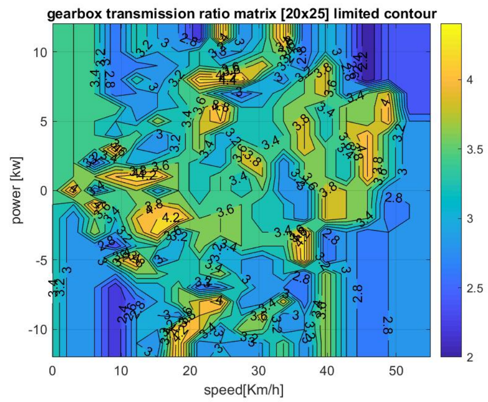

Figure 2.7: τ_g matrix [20x25] contour admissible gears values

In order to obtain a CVT gearbox that is closer to reality, the range in which the transmission operates and a finite number of gear ratios have been defined. The minimum gear ratio is $\tau_{gmin} = 2$, the maximum is $\tau_{gmax} = 4.5$ and among them are 11 other equally spaced gear ratios. Therefore, the matrix's transmissions ratios have been replaced with the closest eligible ones that can be observed in

the contour plot as isolines in figure 2.7.Finally the matrix and its related angular velocity and resistant power vectors have been inserted in the Simulink 2D look up table object, which (as is possible to observe in figure 2.3) for each pair of input ω_{fd} , P_r gives as output the corresponding τ_g.
Also for the gearbox efficiency η_g a look up table has been used but in this case it is 1D and for each gear ratio value corresponds an efficiency value.The efficiency trend of the CVT gearbox in the gear ratio range has been extrapolated from a data-set of efficiency values for the different gears of a manual gearbox designed for an LDV.

2.3 Motor Torque Requirements

In this sub-model the inputs are the torque and angular speed coming out of the gearbox. The aim of this part of the Simulink code, reported in figure 2.8 ,is the evaluation of the peak torque of the electric motor T_m and the required torque T_{req}.

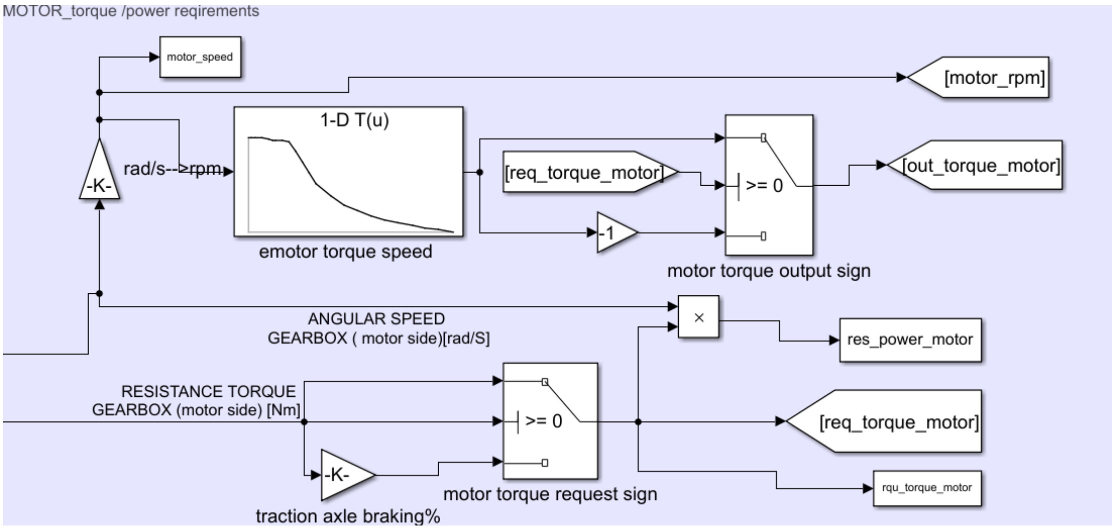

Figure 2.8: Simulink motor torque requirements Sub-model

2.3.1 Torque Required at Motor

For the evaluation of the the T_{req} it is important to consider whether the vehicle is in traction ($T > 0$) or in braking mode ($T < 0$). In fact in the former case the torque required at the gearbox is equal to the torque required at the electric motor; instead in the latter case part of the braking torque is provided by the driving axle and part from the driven axle. In the proposed model the splitting of the braking torque should follow the weight partition between the two axle. It is important to notice that in the driven axle the braking torque is provided only by friction braking at wheels level, whereas on the driving axle part of the braking torque is provided through the transmission by the electric motor working as regenerative brake.Therefore the overall required torque is the sum of these two contribution:

$$T_{req@motor} = \begin{cases} T_g \cdot \%\,weight_{driving\ ax} & \text{for } T_g \leq 0 \\ T_g & \text{for } T_g > 0 \end{cases}$$

2.3.2 Motor Peak Torque

The peak output torque of the electric motor $T_{m\,peak}$ is evaluated using a 1D look up table as function of the angular speed of the motor. In the proposed model it is assumed that the characteristic torque curve is symmetrical and therefore for the same value of speed corresponds the same absolute value of torque whether the electric machine works in traction or in braking.Thus, as can be seen in figure 2.8, the $T_{m\,peak}$ sign is imposed by means of a switch following the trend of the T_{req} sign. In the above mentioned look up table has been inserted the peak motor torque characteristic curve, that together with the mechanical power one, has been derived from the resizing of a more powerful motor map but of the same type (SMPM).To do this, it was necessary to use the mechanical max peak power $P_{m\,peak} = 12kW$ and max rated power$P_{m\,rated} = 6.3kW$ values of the vehicle's technical specifications and the obtained characteristics curves are reported in the figure 2.9.

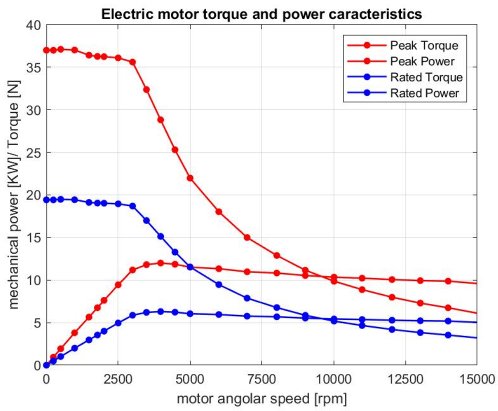

Figure 2.9: Motor Torque and Mechanical Power characteristics curve

2.3.3 Motor Torque

The second part of the Simulink sub-model showed in figure 2.10 aim is the evaluation of the effective torque of the electric motor T_m. This is obtained by comparing the peak torque of the engine with the torque required to run the cycle for each time step.

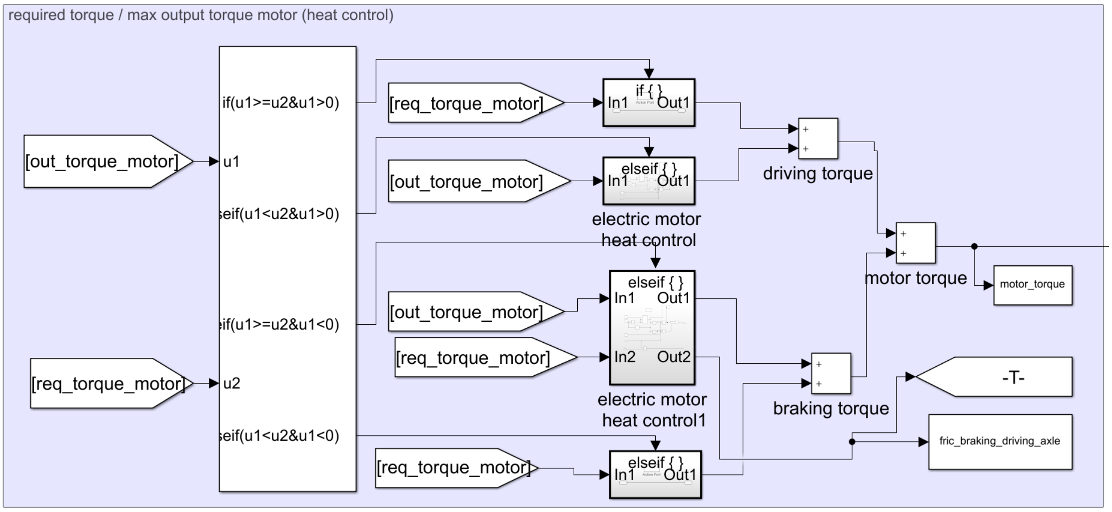

Figure 2.10: Simulink Torque comparison Sub-model

Below are the different cases for the evaluation of the T_m according to the respective $T_{m\,peak}$ and T_{req} values and to the operating mode of the motor:

1. if in absolute value $T_{m\,peak}$ is greater than T_{req} the motor will provide the required torque.
2. Otherwise if in absolute value $T_{m\,peak}$ is less than T_{req} the motor will not be capable of providing the required torque.
   (a) Therefore if it is in traction mode the motor will provide $T_{m\,peak}$ but the vehicle will not be able to follow the driving cycle due to the lower torque capability;
   (b) if instead it is in braking mode the delta torque ΔT will be provided through the friction brake.

$$T_{motor} = \begin{cases} T_{req} & \text{for } |T_{mpeak} > T_{req}| \\ T_m & \text{for } T_{mpeak} < T_{req} \text{ in traction mode} \\ T_{req} = T_m + \Delta T & \text{for } T_{mpeak} < T_{req} \text{ and braking mode} \end{cases}$$

In addition, to avoid overheating of the engine that occur when T_{mpeak} is required for extended periods has been implemented a counter that if the duration of the request of the peak torque overcome $10sec$ reduces the motor peak power to the rated one of $6.3kW$.

2.4 Motor Mechanical and Electrical Power

The inputs of this Simulink sub-model, reported in figure 2.11, are the motor torque T_m and speed ω_m. The aim of this part of the code are the evaluation of the motor mechanical and electrical power respectively $P_{m\,mech}$ and $P_{m\,elec}$.

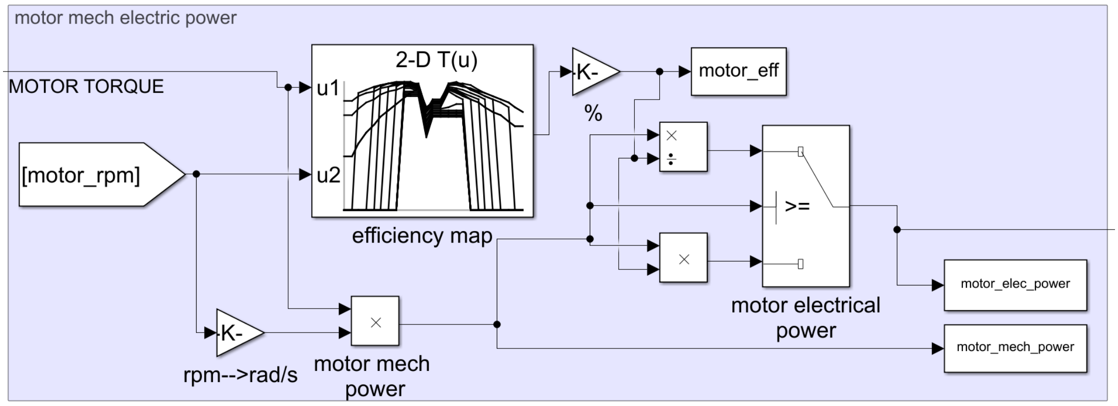

Figure 2.11: Simulink motor Mechanical and Electrical Power Sub-model

The mechanical power of the electric motor is calculated as the product between the torque of the motor and the angular speed of the motor.It is important to note that the electric machine has a limit in the maximum mechanical power it can deliver, but this limitation has already been considered in the torque calculation.

$$P_{m\,mech} = T_m \cdot \omega_m$$

The electrical power of the electric motor is computed multiplying or dividing the mechanical one by the electrical efficiency of the machine η_m depending on the operation mode. In fact, if the efficiency is less than one the power we can recover with the regenerative brake is less than the mechanical one and in case of traction the electric power required by the motor is greater than the mechanical one produced.

$$P_{m\,electrical} = \begin{cases} P_{m\,mechanical} \cdot \eta_{motor} & \text{in braking mode} \\ \frac{P_{m\,mechanical}}{\eta_{motor}} & \text{in traction mode} \end{cases}$$

As It is possible to see from the figure 2.11 the electrical efficiency values are obtained from a 2D Look up table which inputs are the instantaneous torque and angular speed of the motor. As for the motor peak torque the values of η_m as function of T_m and $\omega_m$inserted in the table have been obtained from those for a higher power motor by scaling them. in figure 2.12 and 2.13 are reported contour and 3D plot of motor electrical efficiency map. Unlike the characteristic plot of engine maximum torque and power, the efficiency map is not symmetric, so there are different η_m values for negative and positive power.

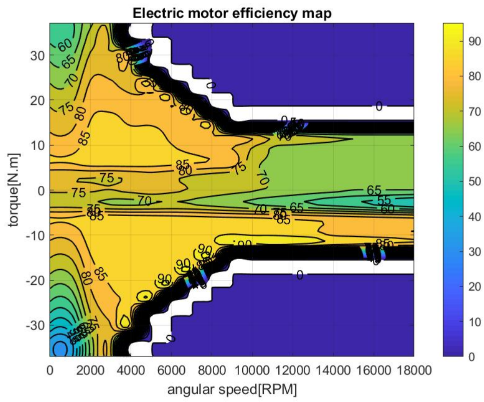

Figure 2.12: η_m matrix contour

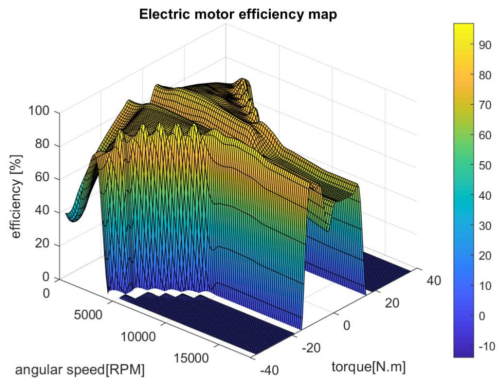

Figure 2.13: η_m matrix 3D plot

2.5 Inverter and Battery

The Simulink sub-models of Inverter and Battery are showed in figure 2.14.The inverter sub-model has as input the motor electrical power $P_{m\,elec}$ and as output the battery electric power P_{batt} that in turns is the input of battery sub-model that at the end give the battery state of charge SOC.

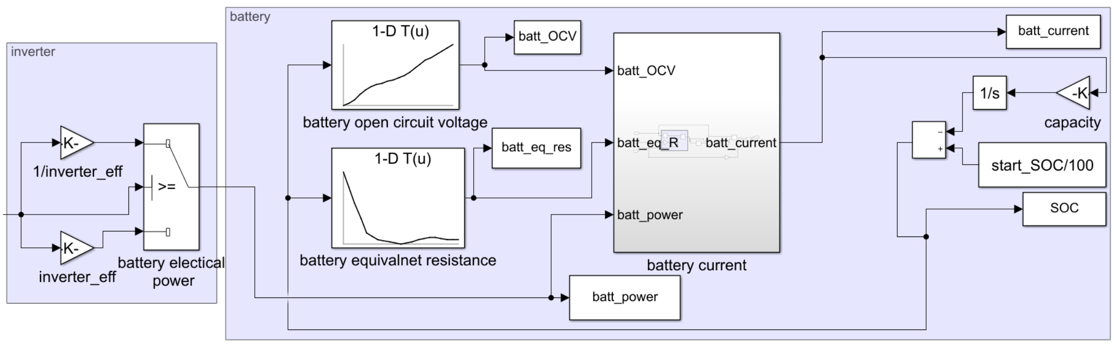

Figure 2.14: Simulink Inverter and Battery Sub-model

2.5.1 Inverter

The inverter sub-model computes the battery electric power staring from the motor electrical power and multiplying or dividing it by the inverter efficiency η_{inv} in a similar way to the motor electrical power calculation:

$$P_{battery} = \begin{cases} P_{m\ electrical} \cdot \eta_{inverter} & \text{in braking mode} \\ \frac{P_{m\ electricel}}{\eta_{inverter}} & \text{in traction mode} \end{cases}$$

The difference is that in this case the efficiency of the inverter is considered constant whit out any dependence on the load.

2.5.2 Battery

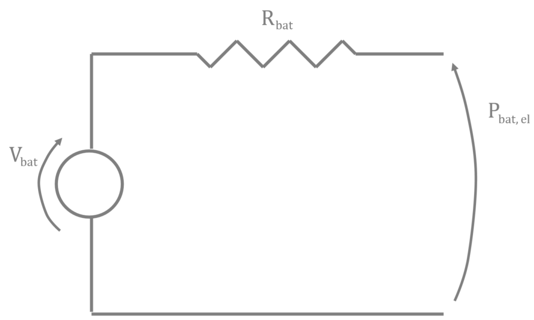

Figure 2.15: Battery equivalent resistant circuit

The battery is modelled as the equivalent resistance circuit reported in figure 2.15, in which the equivalent resistance $R_{eq\ batt}$ and the open-circuit voltage OCV_{batt} of the battery are lumped parameters representing complex chemical process. In the proposed model these two quantities are considered as SOC dependant,instead the effects of temperature variation are neglected i.e. the battery is considered always at constant temperature.

Open-circuit voltage and equivalent resistance

The resistance and the open-circuit voltage of the battery were derived by interpolating the corresponding 1D look up tables showed in figure 2.16 and 2.17, as functions of the battery SOC.

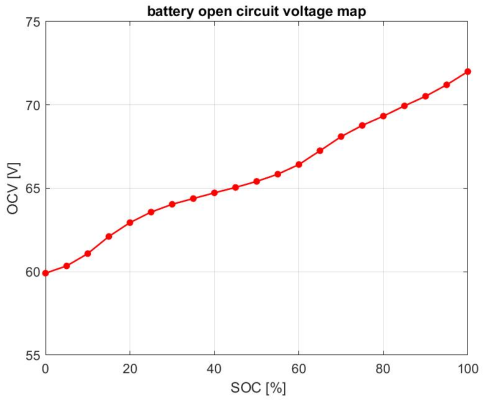

Figure 2.16: Battery Open Circuit Voltage map

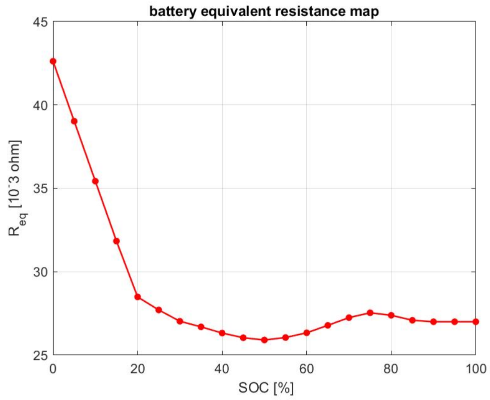

Figure 2.17: Battery equivalent Resistance map

These maps were obtained by scaling curves of a bigger size battery , to do this it was necessary to evaluate the quantities of the battery equivalent circuit ($R_{eq\,batt}$ and OCV_{batt}) for $SOC = 1$ i.e. for battery completely charged.
The vehicle's battery pack code (6-EVF-120) identifies a battery composed of series connected units which characteristics are gathered in table 2.1.

Unit number n_{unit}	6
Voltage OCV_{unit}	$12\ V$
Capacity	$140\ Ah$ @$10hr\ rate\ to$ $1.70\ V$
Weight	$28\ Kg$ with electrolyte
Internal resistance $R_{eq\,unit}$	$\sim 4.5\ m\Omega$

Table 2.1: Battery module characteristics

Therfore the battery $R_{eq\,batt}$ and OCV_{batt} can be computed as the single units values times the number of units that build up the battery pack:

$$R_{eq\,batt} = R_{eq\,unit} \cdot n_{unit} = 27m\Omega$$

$$OCV_{batt} = OCV_{unit} \cdot n_{unit} = 72V$$

current

For each instant of the cycle there is an electrical power request at the battery $P_{batt,elec}$ that could be positive if the vehicle is in traction or negative if It is in braking. Considering a balance of electrical and chemical power of the battery, which is modeled as the equivalent circuit in the figure 2.15, it results that:

$$P_{batt\ chem} = OCV_{batt} \cdot I_{batt} = P_{batt\ elec} + R_{eq\ batt} \cdot I_{batt}^2$$

From this balance is possible to derive the battery current as:

$$I_{batt} = \frac{OCV_{batt} - \sqrt{OCV_{batt}^2 - 4 \cdot R_{eq\ batt} \cdot P_{batt\ elec}}}{2 \cdot R_{eq\ batt}}$$

The maximum power of the battery is derived from the value of the maximum current, the current for which the root in the previous equation is null:

$$P_{batt\ elec\ max} = \frac{OCV_{batt}^2}{4 \cdot R_{eq\ batt}}$$

state of charge

The SOC represents the electrical status of the battery and depends on the equivalent battery capacity C_{batt} and the flowing current I_{batt}, as follows:

$$SOC = SOC_0 - \int \frac{I_{batt}}{c_{batt}} dt$$

SOC reduces when the vehicle is in traction but can be also restored tanks to regenerative braking.

2.6 Vehicle speed

The aim of this last Simulink sub-model, sowed below in figure 2.18, is to evaluate the "real speed" that the vehicle assumes during the cycle. In fact, from the speed of the cycle, the torque required from the engine has been calculated, but if the peak torque that this can provide is lower, the vehicle speed will be different from that set.

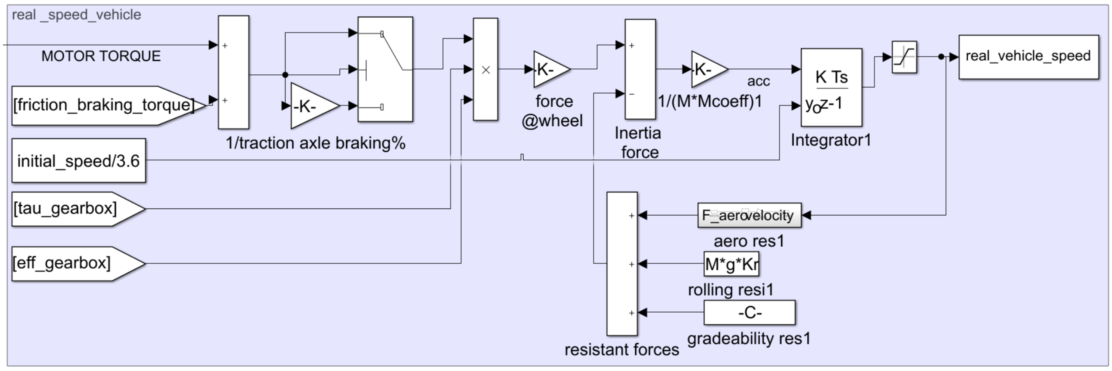

Figure 2.18: Simulink vehicle speed Sub-model

2.6.1 Traction and Braking forces at wheels

The model inputs are the motor torque T_m (that includes both driving and regenerative braking) and the friction braking torque on the driving axle ΔT. The sum of these two torque gives the total torque applied on the driving axle at motor level that which is then transmitted at wheel level and converted in force dividing it by the rolling radius :

$$T_{driving\ ax} = (T_m + \Delta T) \ \text{ @ motor level}$$

$$T_{driving\ ax} = (T_m + \Delta T) \cdot (\tau_g \cdot \eta_g) \cdot (\tau_{fd} \cdot \eta_{fd}) \ \text{ @ wheel level}$$

$$F_{driving\ ax} = \frac{T_{driving\ ax}}{r_d}$$

To obtain the total force at the wheels F_{wheel}, the braking force applied to the driven axle must also be taken into account. This contribution is added to the driving axle braking force by dividing this last one by the driving axle weight distribution.

$$F_{wheels} = \begin{cases} F_{driving\ ax} & \text{in traction mode} \\ F_{driving\ ax} + F_{driven\ ax} = \frac{F_{driving\ ax}}{\%\, weight_{driving\ ax}} & \text{in braking mode} \end{cases}$$

2.6.2 Balance of forces at wheels

In the opposite way to the Resistant Power sub-model in which the resistant force has been calculated from the speed now the real vehicle speed is calculated from the force available at the wheels. Are also taken into account the resistances to the vehicle motion ,that are: Rolling ,Grade, Aerodynamic and Inertia. At this point it is possible to write the balance of all forces to the wheel as:

$$F_{wheels} - F_r - F_g - F_a = F_i$$

The vehicle acceleration can be computed dividing the Inertia force by the apparent translating mass of the vehicle, and finally integrating it the "real" speed is also obtained.

$$V_{real} = \int \frac{F_i}{M_a t}$$

The model needs a feedback in fact, before it can calculate the speed, it must estimate the aerodynamic resistance that is a function of the speed.

Chapter 3

Model parameter selection and firsts simulations

3.1 Model parameters

Once the model has been built, in addition to the speed profile, the various sub-models need additional data to run the simulations.

3.1.1 Vehicle technical specification

The information available on the vehicle are reported below in table 3.1.

Some of the vehicle technical specification data have already been used to define the look up tables used in the model, such as in section 2.3.2, where P_{peak} and P_{rated} have been used to resize the electric motor torque characteristics. Instead for what concerns section 2.5.2, to obtain the look up table of the OCV_{batt} and $R_{eq\,batt}$ function of battery SOC,have been used additional data, reported in table 2.1,which have been founded using the known battery code.

3.2 First approximation of model parameters

In this section the values of the model parameters have been decided in order to compile the first simulations. However, for the evaluation of these parameters the information available on the vehicle is not enough , so when data are not available, attempts have been made to provide plausible values from other vehicles in the same category or making assumptions:

1. **vehicle mass** (m)
   The mass of the vehicle for the homologation test is the kerb mass to which

Vehicle technical data		
Vehicle homologation class		L7e
$m_{bodywork}$	Kerb weight without powertrain $[kg]$	650
V_{max}	Max speed $[km/h]$	50
$\%_{weight_{driving\ ax}}$	driving axle weight distribution	54%
Dimensions:		
l	Length $[mm]$	2830
w	Width $[mm]$	1500
h	Height $[mm]$	1565
h_{gc}	Minimum ground clearance $[mm]$	1565
Electric Motor (SMPM):		
P_{peak}	Peak power $[kW]$	12
P_{rated}	Rated power $[kW]$	6.3
Battery (6-EVF-120A):		
V_{batt}	Battery voltage $[V]$	72
C_{batt}	Battery capacity$[Ah]$	140

Table 3.1: Vehicle technical specification

is added that of the driver (m_{driver}) which as standard is considered $70kg$. In turn, the kerb mass is calculated as ($m_{bodywork}$) adding the weight of the powertrain ($m_{powertrain}$), i.e. about $20kg$ and the weight of the battery which is calculated from the weight of the single module ($m_{batt_{unit}}$).

$$m = m_{bodywork} + m_{powertrain} + m_{batt_{unit}} \cdot n_{unit} + m_{driver} = 650 + 10 + 28 \cdot 6 + 70 = 898kg$$

2. **rolling friction coefficient (K_r)**
   In this model it has been decided to use a rolling resistance formulation so the K_r coefficient is constant, however it is not easy to find the proper value which is in any case a function of the type of tyre and the surface on which it moves. As a first approximation, following the study [(Daniciu) 5, (2016)] concerning the electrification of a vehicle with similar characteristics, it was decided to assign the same value to the rolling resistance coefficient.

$$K_r = 0.002$$

3. **rolling radius (r_d)**
   Having no information on the radius of the wheels of the vehicle, was taken as a reference that of the Renault Twizy which is a quadricycle of the same category. Found the tire sidewall marking of the Twizy (125/80R13), it is possible to calculate the wheel radius. The rolling radius is slightly smaller due

to the deformation caused by the weight of the vehicle and is approximately 97% of the wheel radius.

$$r_d = \left(125 \cdot \frac{80}{100} + 25.4 \cdot \frac{13}{2}\right) \cdot 97\% \div 1000 = 0.257m$$

4. **frontal area** (A_f)
   The projected frontal area is approximated by considering simple geometric figures as seen in figure 3.1 in function of the measures of vehicle height (h), width (w), ground clearance (h_{gc}) and tyre width (w_{tyre}).

   $$A_f = w\cdot(h-h_{gc})+2\cdot h_{gc}\cdot w_{tyre} = (1500\cdot(1565-165)+2\cdot 165\cdot 125)\div 10^6 = 2.14m$$

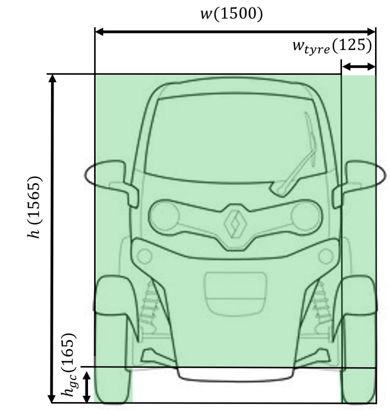

Figure 3.1: Vehicle frontal area

5. **drag coefficient** (C_x)
   As in the case of the rolling radius, having no information on the aerodynamic drag coefficient of the vehicle, the one of Renault Twizy is used. The value is higher than the average value of current vehicles, but for a quadricycle designed for a maximum speed of $50km/h$ the aerodynamic resistance is of secondary importance.

   $$C_x = 0.65$$

6. **transmission ratios and efficiencies** (τ_{fd} τ_g η_{fd} η_g)
   The transmission ratio of the final drive has been set to one of the most frequently used values, and even if it were wrong thanks to the method used in section2.2.1 to define the transmission values of the gearbox, it would be compensated. In fact, the product of the two gear ratios is equal to the overall transmission ratio calculated from the ratio between the angular speed of the

engine and that of the wheels. The efficiencies have been assigned reasonable values, moreover, that of the final drive is constant, while that of the gearbox varies in a range depending on the gear ratio.

$$\tau_{fd} = 3.6 \quad 2 \leq \tau_g \leq 4.5 \quad \eta_{fd} = 0.97 \quad 0.97 \leq \eta_g \leq 0.98$$

7. **inverter efficiency** (η_{inv})
   In this case, too, since there is no information on the efficiency of the inverter, it was decided to assign it a constant value.

$$\eta_{inv} = 0.95$$

8. **Auxiliaries** (AUX)
   Due to the low power of the vehicle, the importance of consumption due to the auxiliaries is not negligible and can greatly affect the SOC of the battery and therefore the range of the vehicle. Assuming the vehicle's air conditioning system is switched off during the tests, the main source of consumption is to be found in the headlights.Taking as reference the Renault Twizy it is possible to find the power consumption of the light bulbs of the two pairs of headlights: the main ($2 \times 55/70W$) and side ones ($2 \times 5W$).

$$AUX = 2 \cdot (60 + 5) = 130W$$

In the following table 3.2 are summarized all the parameters necessary to run the model: those coming from the technical information of the vehicle,those just estimated, and also the range of those evaluated in the code from the Look up tables.

Model parameters	
Battery capacity	$C_{batt} = 140\ Ah$
Battery voltage	$60 \leq OCV_{batt} \leq 72\ V$
Battery equivalent resistance	$26 \leq R_{eq\ batt} \leq 42\ m\Omega$
Battery initial state of charge	$SOC_0 = 1$
Air density	$\rho = 1.25\ kg/m^3$
Gravity acceleration	$g = 9.81\ m/s^2$

Table 3.2: First approximation model parameters

3.3 Homologation cycles Simulations

Once all the parameters of the model have been set, the first simulations are made by imposing as input the speed profiles of the homologation tests. In order to

Model parameters	
Vehicle mass	$m = 898kg$
Apparent translating mass coef.	$C_{at} = 1.05$
Driving axle weight distribution	$\%_{weight_{driving\ ax}} = 54\%$
Slope	$\alpha = 0\ deg$
Rolling friction coef.	$K_r = 0.002$
Rolling radius	$r_d = 0.257\ m$
Frontal area	$A_f = 2.14\ m$
Drag coef.	$C_x = 0.65$
Final drive transmission ratio	$\tau_{fd} = 3.6$
Final drive efficiency	$\eta_{fd} = 0.97$
Gearbox transmission ratio	$2 \leq \tau_g \leq 4.5$
Gearbox efficiency	$0.97 \leq \eta_g \leq 0.98$
Motor peak torque	$T_{m\ peak} = 37\ Nm$
Motor electric efficiency	$0.3 \leq \eta_m \leq 0.9$
Auxiliary power request	$aux = 130\ W$
Inverter efficiency	$\eta_{inv} = 0.95$

ascertain its behaviour, it was decided to test the model with the ECE, which is a representative cycle of urban driving condition and the EUDC, which instead represents an extra-urban driving.

3.3.1 ECE simulation results

The vehicle designed for urban driving should be able to simulate the ECE cycle without any problem, in fact as can be seen in Figure 3.2 the vehicle speed completely overlaps the speed cycle and the same applies to the mechanical power demand at the motor.

Since the ECE cycle is characterized by low speeds ($< 50\ km/h$) and low powers, it can be noticed in figure 3.3 that all the working points of the engine are within the torque peak map. Moreover, figure 3.4 representing the engine efficiency map shows that throughout the cycle the engine always works within regions having a very high efficiency always higher than 65%.

The Graphs in figure 3.5 represent how the CVT gear ratio varies over the cycle (around an average value of 3.4) in order to keep the engine working point at a high efficiency around 80 and the angular speed of the motor below $5000rpm$. These graphs confirm that the CVT gearbox, simulated by the look up table obtained from analysis of experimental data, behaves in a reasonable way. In figure 3.6 can

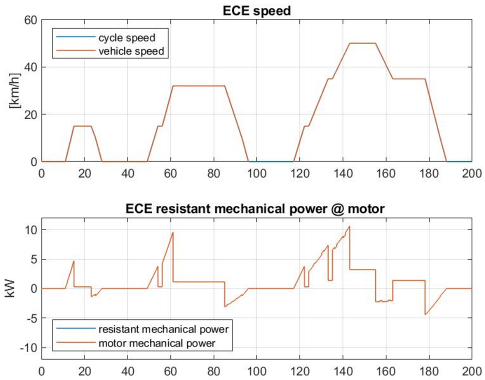

Figure 3.2: ECE cycle speed and resistant power @ motor

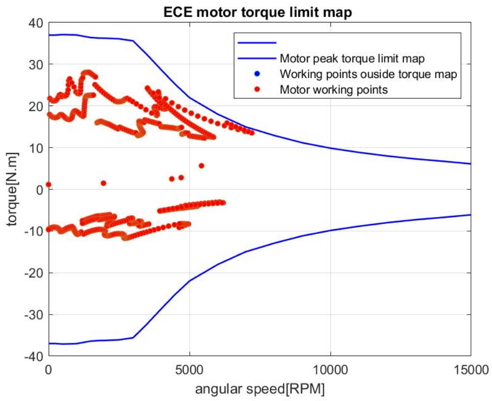

Figure 3.3: ECE cycle working points on motor torque map

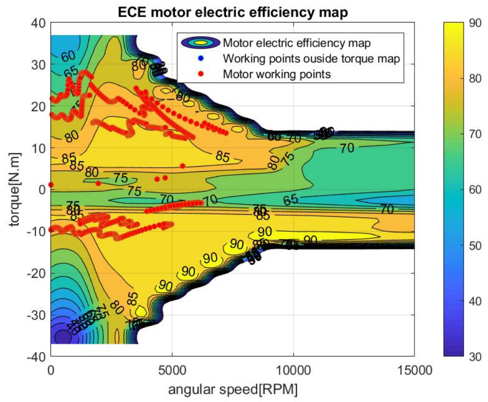

Figure 3.4: ECE cycle working points on efficiency map

be observed the power request for different section of the model power flow. In the upper graph the mechanical and electrical power at motor are compared, it can be seen that in traction mode $P_{m\ mech} < P_{m\ elet}$ while in regenerative braking one is the opposite. In addition, the ratio between these two powers is not constant in fact η_m varies along the cycle. In the lower graph the electrical powers at motor and at battery are compared, as in the previous case, in traction mode $P_{m\ elet} < P_{batt}$ while in regenerative braking one is the contrary. Unlike the previous case the ratio between the two powers remains the same throughout the cycle in fact η_{inv} has a constant value.

Finally, figures 3.7 and 3.8 show the $R_{eq\ batt}$, OCV_{batt}, I_{batt}, and SOC trends of the battery. Given the low energy demand of the ECE cycle, the variation of SOC is

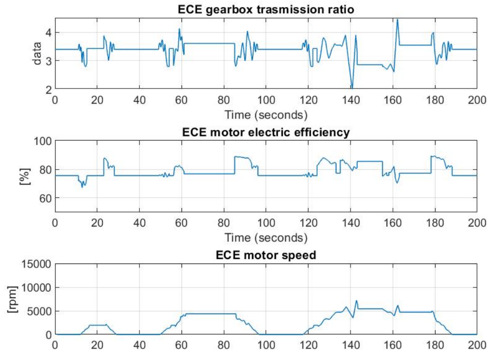

Figure 3.5: ECE cycle motor and gearbox behaviour

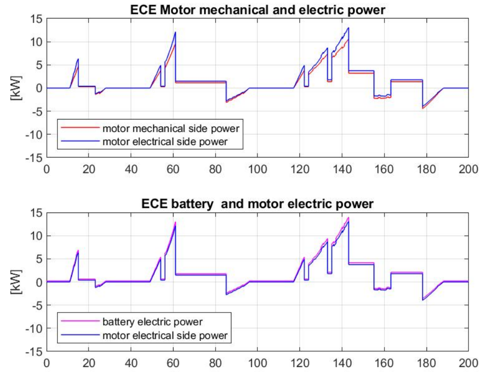

Figure 3.6: ECE cycle mechanical and electrical powers

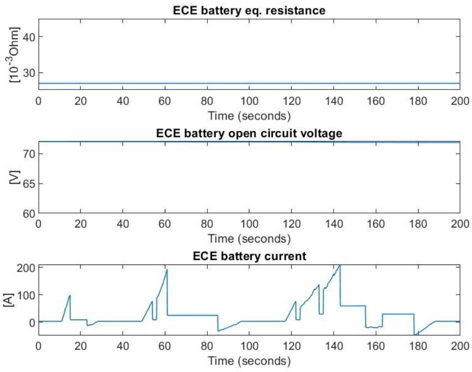

Figure 3.7: ECE cycle battery behaviour

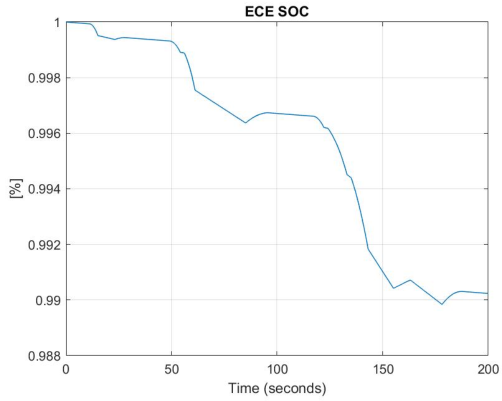

Figure 3.8: ECE cycle battery SOC

minimal and consequently also that of $R_{eq\,batt}$ and OCV_{batt} which are its function, instead the I_{batt} follows the trend of the electric power of the battery and assumes negative values when the vehicle is in regenerative braking condition.

3.3.2 EUDC simulation results

The model has been simulated also along the EUDC cycle which, being representative of an extra-urban driving, is characterized by higher speeds and therefore by a higher power demand.

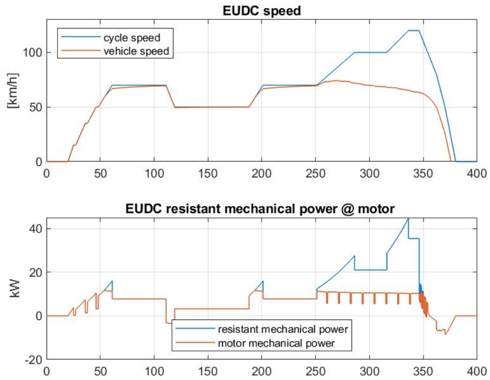

Figure 3.9: EUDC cycle speed and resistant power @ motor

As can be seen in the figure 3.9 the simulated vehicle, which is designed for a maximum speed of $50km/h$, can not follow the cycle EUDC whose maximum speed is $120km/h$.Moreover, from the power graph it can be seen that in the last part , corresponding to the peak of maximum speed, the trend of the mechanical power supplied by the motor is inconstant, i.e. there are steps. This trend is due to the overheating control of the engine defined in the model in section2.3.3. This acts on the motor when it delivers the maximum power for a time interval longer than $10sec$ reducing the power from the peak one to the rated one, with the aim of avoiding overheating.

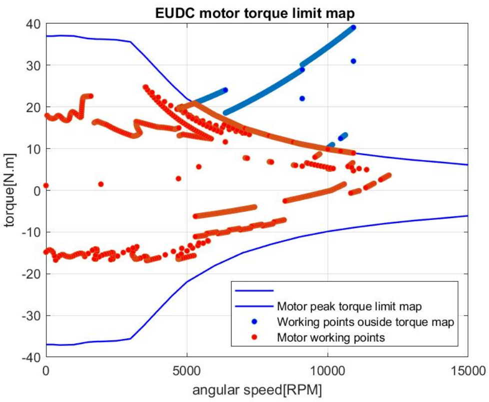

Figure 3.10: EUDC cycle working points on motor torque map

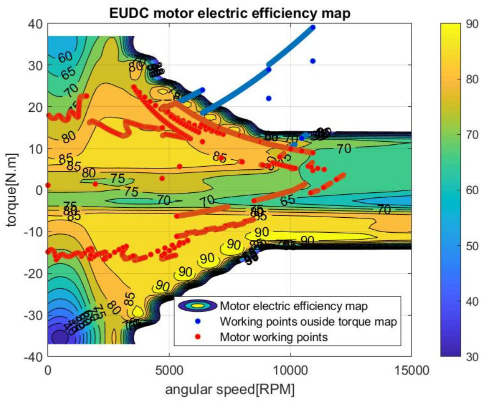

Figure 3.11: EUDC cycle working points on efficiency map

The figures3.10 and 3.11 show that some of the working points at which the engine should work in order to respect the speed cycle fall outside the maximum engine peak torque limit, but for the points falling within the map the engine efficiency is quite high.

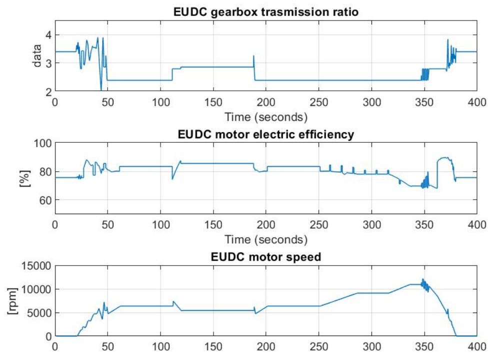

Figure 3.12: EUDC cycle motor and gearbox behaviour

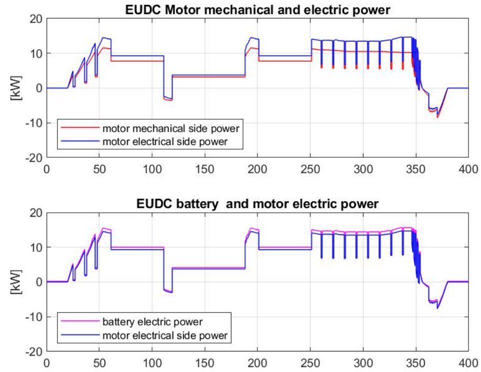

Figure 3.13: EUDC cycle mechanical and electrical powers

These last graphs represent the electrical power required by the vehicle which, being greater than the ECE cycle one, lead to a greater reduction of SOC of the battery and consequently of the $R_{eq\ batt}$ and OCV_{batt} shown in the figure 3.14 and 3.15.

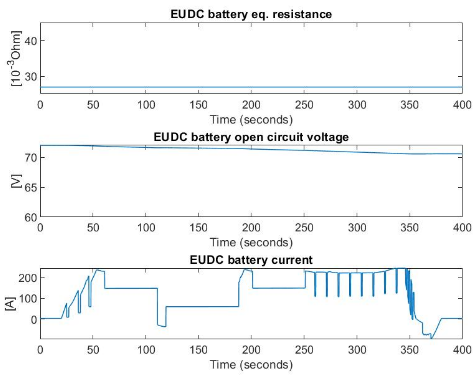

Figure 3.14: EUDC cycle battery behaviour

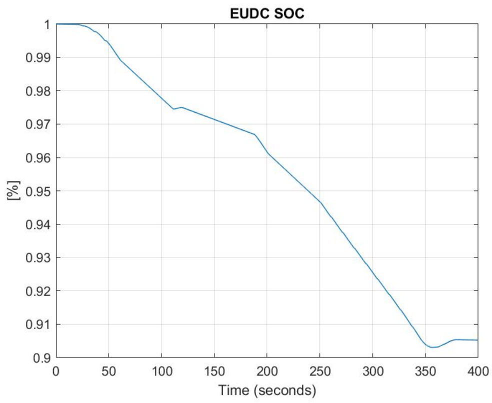

Figure 3.15: EUDC cycle battery SOC

Chapter 4

Model verification

Thanks to simulations on homologation cycles, it has been confirmed that the model meets the capabilities of the vehicle, in fact it is able to cover the urban cycle but not the extra-urban one. This chapter will instead take into consideration the experimental cycles, i.e. cycles actually travelled by the vehicle during which data were collected. For every second of the duration of these driving missions, the sensors with which the vehicle is equipped have collected information about: GPS position, vehicle speed, engine angular speed and battery SOC. Therefore the purpose of these simulations will be to verify the behavior of the model more than in terms of capacity to travel the cycles, in terms of energy consumption. This verification will be carried out by a comparison between the battery SOC simulated by the model at the end of the cycle e the measured one by the vehicle during the driving mission.

4.1 Experimental cycle speed profile data

For these simulations the input parameters of the model are the same as those used for the homologation cycles shown in Table 3.2 except for the initial SOC value of the battery which will be the same as the one measured at the beginning of the driving mission. In addition, the speed profile must be extrapolated from the data collected by the sensors.
Figure 4.1 shows two velocity graphs relative to an experimental cycle, the first plot calculated from the GPS sensor data and the second from the speed sensor. As can be seen for the chosen cycle (but the same thing applies to the others) the speed signal from the GPS contains much more noise than the other. This is due to the inaccuracies of the measurement and also to the fact that the speed was obtained indirectly as a derivative of the distance between the adjacent positions defined by the latitude and longitude measured by GPS. Instead with regard to

the speed sensor the velocity is measured directly, so the noise and uncertainty are lower however the resolution of the measurement is very low in fact it is to the units.

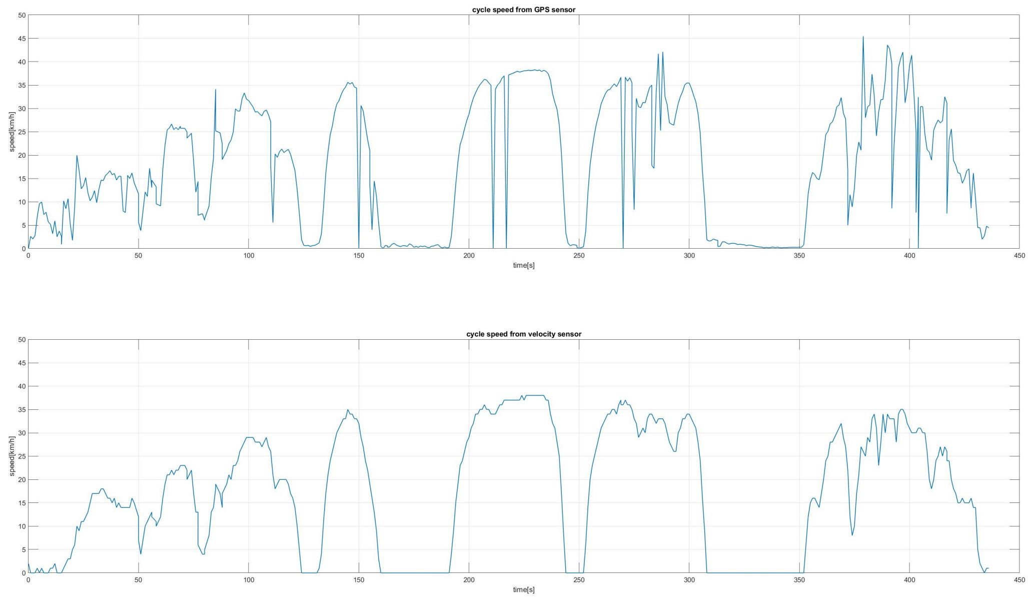

Figure 4.1: Experimental cycle speed profile data from GPS and velocity sensors

4.1.1 selection of the appropriate filter

It was decided to use the less noisy signal, i.e. the one obtained from the speed sensor, and tried to improve it usinfg a filter.The following filters have been taken into account:

1. **Moving average filter**
   The moving average filter is a simple low-pass FIR (Finite Impulse Response) filter that is commonly used to attenuate the short term fluctuation of the signal, Given a data set and a fixed subset size ($windowsize$), the first filtered element element is obtained by taking the average of the initial subset. Then the procedure is repeated sliding the window along the data set until reach the last element.The following equation defines a simple moving-average filter of a vector x:

$$y(n) = \frac{1}{windowsize} \cdot [x(n) + x(n-1)... + x(n-(windowsize-1))]$$

2. **Hampel filter**
   The Hampel filter is used to identify and replace outliers in a given series. It uses a sliding window over the number series that is centered on the sampled element, for each one of these elements estimate the standard deviation (σ) about its window median using the median absolute deviation. If a sample differs from the median by more than x times the standard deviations , it is replaced with the median.

3. **Savitzky-Golay filter**
   The Savitzky-Golay filter, that is well described in article [6], can be used to smooth a signal, using a method based on local least-squares polynomial approximation. Given a data set and a fixed subset size ($windowsize$) it fits a polynomial which order is lower than the window dimension, then using least square method is able to calculate the polynomial coefficients and replace the central data with the one evaluated by the polynomial.

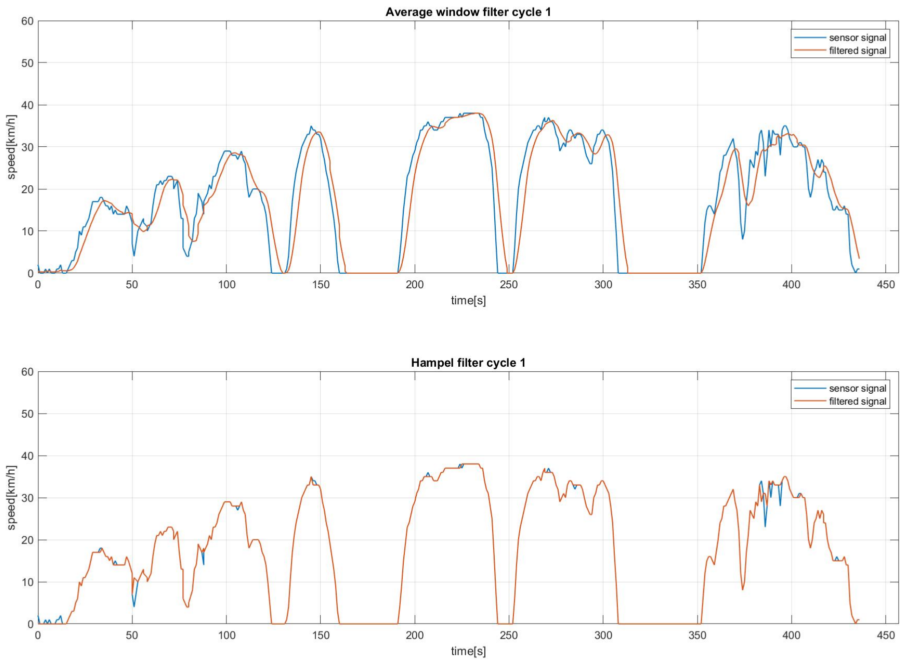

Figure 4.2: Filtered experimental speed profile velocity sensors

In figure 4.2 are reported the graphs of the speed signal filtered using two of the the above presented methods: the first one was obtained with the moving average setting the window size equal to 7 and the second one with the Hampel filter

whit the same dimension of the window size and a threshold value for outliers identification equal to $(1.5 \cdot \sigma)$.
As it is possible to see the moving average filter returned a speed profile too much attenuated in fact, in addition to eliminating the noise and smooth the signal it also loses the general trend of the velocity and causes a time shift. The Hampel filter, on the other hand, eliminates some of the outliers but does not soften the signal.
In the choice of the filter that will be used for the simulations it must be considered that the speed signal is obtained through a sensor whose sensitivity is to the units. Therefore the signal has a stepped pattern that must necessarily be softened otherwise the resulting step accelerations would exceed the capabilities of the vehicle and the model would not be able to follow the cycle. At the same time the filtered signal must be representative of the original speed cycle to have a comparison between the energy estimated by the model and the energy used by the vehicle to run the cycle. For these reasons the two filters proposed above have been discarded and the Savitzky-Golay filter has been chosen. This one thanks to the use of the polynomial function can follow the trend of the original signal and at the same time to soften the step-growth and peaks.

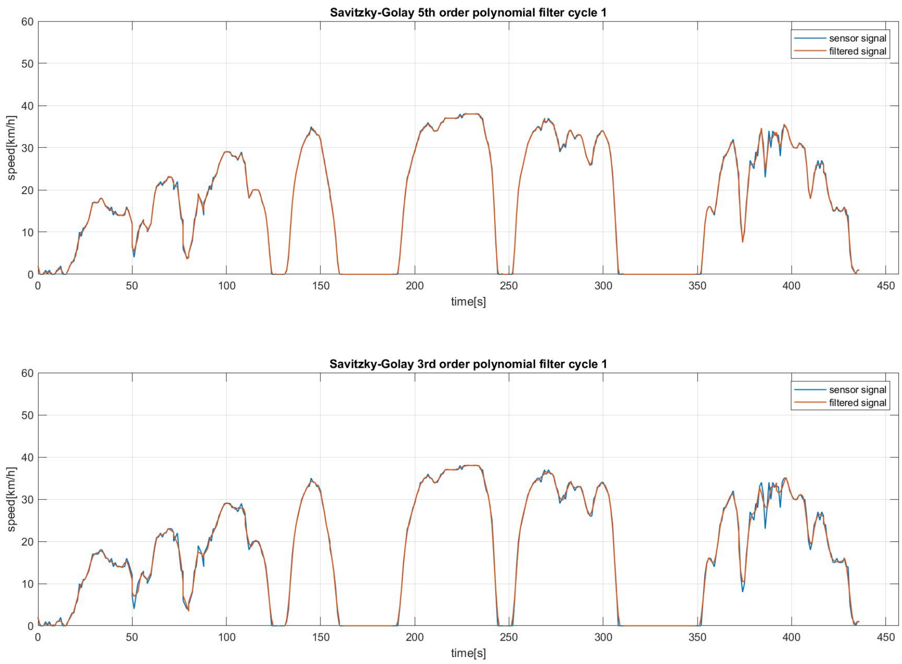

Figure 4.3: Filtered experimental speed profile velocity sensors using Savitzky-Golay method

Figure4.3 shows two graphs of the speed profile filtered using this method with a window of the same size but respectively 5^{th} and 3^{rd} degree polynomials. Observing them can be noticed that using a high degree polynomial the filtered signal will remain more adherent to the original instead the low degree one will lead to neglect of the sudden peaks. The most appropriate grade to be used in the filter must be chosen as a trade-off between adherence to the original signal and peak attenuation. To see the behavior of the model and its results is been simulate the same experimental cycle with the two approximations.

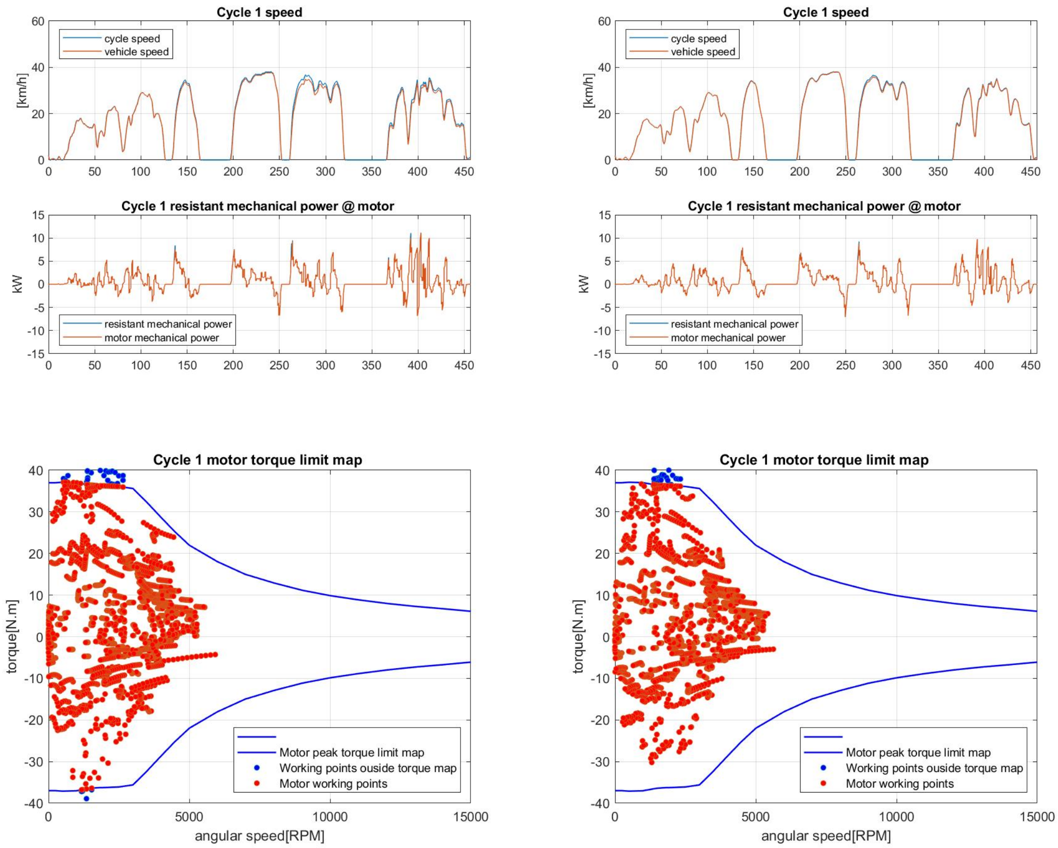

Figure 4.4: Experimental cycle results obtained using Savitzky-Golay filter with different polynomial degree

Figure 4.4 shows on the left the results obtained by approximating the signal using the polynomial of 5^{th} degree and on the right those obtained with one of 3^{rd} degree. In the first case the simulated vehicle is not able to follow the cycle profile due to some very strong power peaks, instead in the second case the speed follows the cycle much better. Moreover thanks to the smoothing of the cycle in the second

case the engine working points that fall outside of the maximum torque map are much less.
Finally, it can be observed that the differences in the two filtered speed profiles are very small and therefore the total energy to run them is almost identical. Therefore, considering the purpose of the model is to obtain an estimate of the energy consumed by the vehicle, it was decided to use the filter with the 3^{rd} degree polynomial. In fact this filter using a polynomial of lower degree maintains the general trend of the power reducing only the instantaneous fluctuation that has a negligible effect on the calculation of energy but allowing a better behavior of the model.

4.2 Experimental cycles first simulations

Simulations of experimental cycles require the parameters of the model and the speed profiles of the cycles. The first ones have been defined and verified through the simulations of the homologation cycles that have given good results so also in this case will be maintained the same. The second ones are obtained from the signal measured by the sensor of the vehicle through a filter. The right filter has been defined in the previous chapter after careful analysis and verification.
In the previous subsections the results on *cycle*1 were always shown, because it is one of the shortest and this allowed a better view of the speed trend. However, now having to analyze not only the capacity of the vehicle to follow the cycle but also the consumption, the results of cycle 1 will be accompanied by those of other cycles that are longer and therefore provide better information about the energy needed to run them.

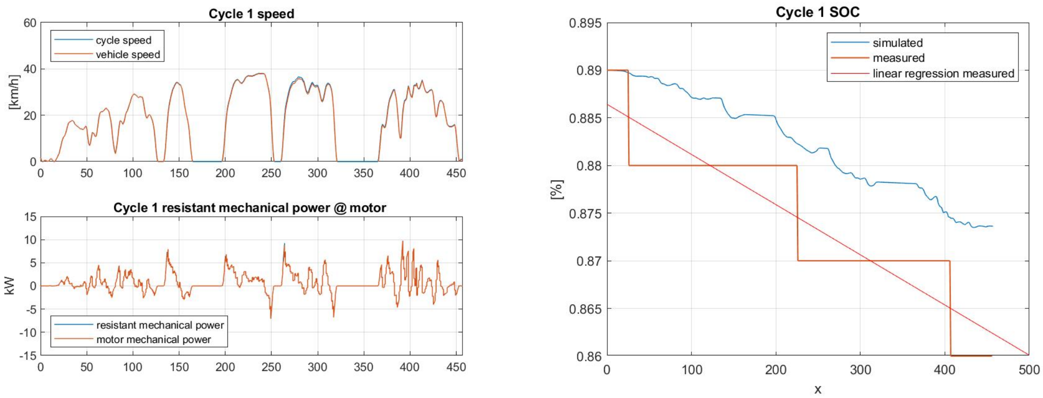

Figure 4.5: Experimental cycle 1 results: mechanical power and SOC

Figure 4.5 shows the results of the simulation of cycle 1: the graph of the speed and mechanical power was reported only as confirmation that the model can follow the cycle, but the interesting result is the SOC of the battery. The graph shows the SOC obtained from the simulation and the one measured by the vehicle. The latter is provided with a low resolution so its linear regression has also been graphed to facilitate the comparison with the simulated values. Analyzing this graph it seems that the trend of the two SOCs is divergent although they start from the same value, the simulated consumption is lower than the one measured.
The difference in simulated and measured consumption is accentuated in longer cycles such as those shown in Figure 4.6 where the SOC curves will be even more divergent.

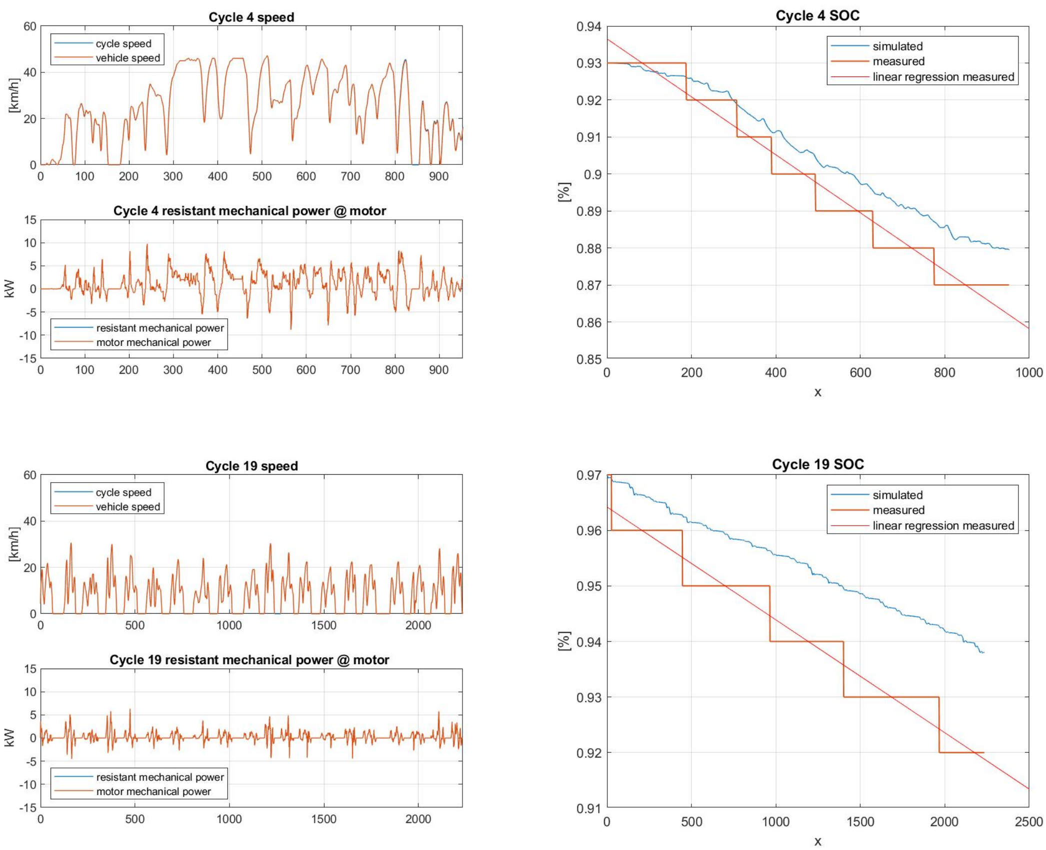

Figure 4.6: Experimental cycles 4 and 19 results: mechanical power and SOC

The tendency of the model to underestimate the power consumption and therefore the SOC of the battery was found in addition to the above cycles in almost all simulated cycles.

4.3 Sensitivity analysis

Having found the problem of the model in the underestimation of the energy required to run the cycle, it was decided to vary some of the parameters decided previously and gathered in table 3.2 and observe the effect on the result of the simulations. Given the lack of data on the vehicle, the majority of these were estimated by other vehicles or by making assumptions. The parameters that have been modified are:

- The **coefficient of rolling friction** (K_r) that had been set in initially at 0.002 in following the decision taken by Daniciu in his project on a vehicle with similar characteristics. It was chosen to vary this parameter because it is directly proportional to Rolling resistance, and considering the average speed of the vehicle, it has an important influence on the total resistance. Besides, the coefficient can typically assume a wide range of values, just think that on asphalt the typical value for bicycle tires is 0.002 and for those of a car is $0.01 - 0.015$. The value used initially was very small and equal to that typically used for a bike so it was decided to increase it.

- The **electric auxiliaries** (AUX) that are powered through the inverter from the battery. The auxiliary's value was initially set to $130W$ which is the power consumption of the headlights of the Renault Twizy. Therefore having no real information about the auxiliary devices of the vehicle and the magnitude of their impact on the SOC it was decided to increase the value.

The set of values assumed by these two parameters for the sensibility analysis are the following:

$$K_r = \ [\ 0.002\ 0.004\ 0.006\ 0.008\ ]$$

$$Aux = \ [\ 130\ 200\ 250\ 300\ ]\ W$$

Sensitivity analysis was performed by simulating all possible combinations of the values that these two parameters assume the above reported figures 4.7, 4.8and 4.9 shown the results of these simulation of the previously considered experimental cycles.

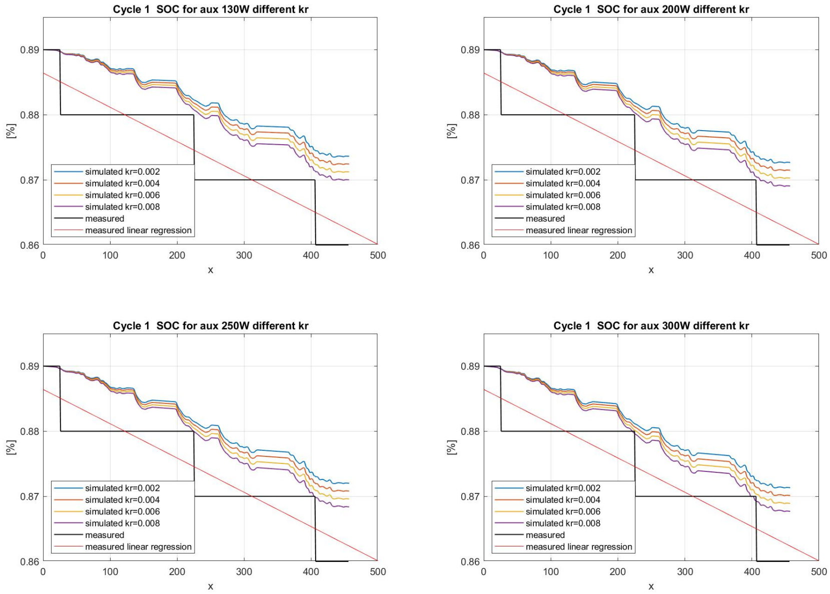

Figure 4.7: Sensitivity analysis experimental cycle 1

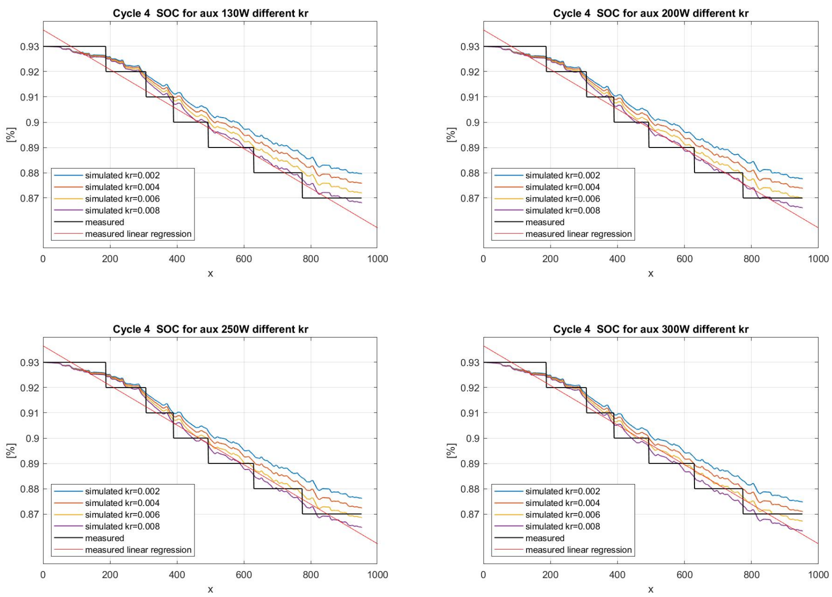

Figure 4.8: Sensitivity analysis experimental cycle 4

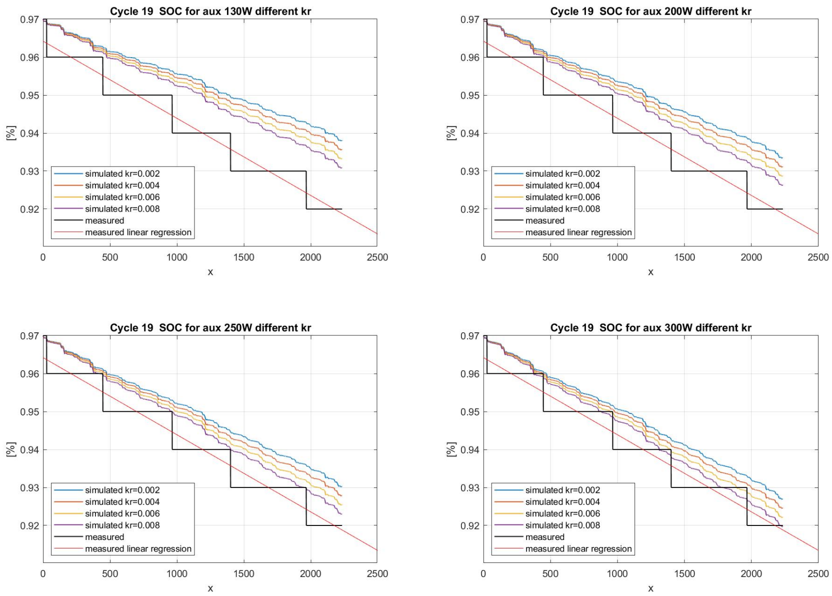

Figure 4.9: Sensitivity analysis experimental cycle 19

From these results it can be deduced that the variation of rolling resistance coefficient has a preponderant effect on the SOC compared to the auxiliaries. For almost all cycles the simulation results closer to the experimental ones are obtained by increasing the consumption, however, given the poor resolution of the experimental signal, it is difficult to define which is the best set of parameters. For example, by analyzing the graphs of the cycles shown here we notice that:

- for the cycle 1 could be right both the trend of the soc simulated with ($K_r = 0.008$ and $Aux = 250$) and the one obtained with ($k_r = 0.006$ and $Aux = 300$).
- for cycle 4 instead the two sets of parameters that give a SOC that matches the signal one are ($K_r = 0.006$ and $Aux = 200$) and ($k_r = 0.004$ and $Aux = 300$).
- lastly, for cycle 19, the best fits are obtained using ($K_r = 0.008$ and $Aux = 250$) and ($k_r = 0.008$ for $Aux = 300$).

Finally, to obtain a good compromise between all the results of the experimental cycles, the value of the parameters has been set as:

$$K_r = 0.006 \;\; and \;\; Aux = 200$$

.

At this point the model is considered verified because the few data available on the vehicle and the low resolution of the measurements obtained during road missions, do not allow to further improve the model or refine simulation parameters.The final results of all other experimental cycles simulated using the proposed model and the parameters which have so far been defined are listed in the Appendix.

Chapter 5

Energy efficiency test procedure for L7 category vehicles

In this last chapter, it is defined a specific procedure for the evaluation of energy consumption and the range of BEVs belonging to category L7, starting from the road test data and model results.

5.1 Emission test cycle definition

The driving cycle is a fundamental element of the test procedure because the energy consumption of the vehicle is directly related to the operating condition of the motor.Therefore, to obtain plausible consumption values the cycle must be a reliable representation of the real driving conditions of the vehicle category to which it refers.The best way to define the cycle is therefore to rely on the data obtained during the road test of the electric quadricycle.
The speed profiles previously filtered using the Savitzky-Golay method were analyzed to obtain statistical values representative of road missions. After which, to obtain reference values for the test cycle definition, the median between all the experimental cycles of the quantities considered has been calculated and collected in the fist column of Table 5.1.The cycle for the emission test was generated by combining fragments of the experimental speed profiles. These were chosen to obtain an initial part characterized by lower speeds, a central part more dynamic and a final part with higher speeds. The cycle thus generated is represented in Figure 5.1 and the same quantities previously calculated for the experimental speed profiles are shown in the second column of Table 5.1.

	median values of experimental cycles	**proposed emission cycle**
max speed $[\frac{km}{h}]$	44	51
mean speed $[\frac{km}{h}]$	17	21
max acceleration $[\frac{m}{s^2}]$	1.79	1.59
mean acceleration $[\frac{m}{s^2}]$	0.25	0.22
max deceleration $[\frac{m}{s^2}]$	-2.2	-2.42
mean deceleration $[\frac{m}{s^2}]$	-0.24	-0.20
distance $[km]$	4.3	8.6
duration $[s]$	888	1192
idle time $[\%]$	20	11

Table 5.1: Representative quantities of speed profiles

The data in the table shows that :

- In the cycle, attention has been paid to maintaining the median values of the experimental data concerning acceleration and deceleration, considering these as the parameters that most characterize the urban driving conditions.
- On the other hand, concerning the duration and the distance covered, it was decided to increase them to obtain more reliable results.
- Finally, also the velocity has been increased to be able to take into account the working conditions for the maximum speed of the vehicle

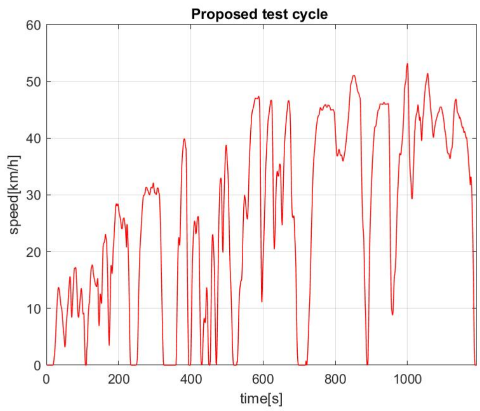

Figure 5.1: Proposed test cycle

5.1.1 Proposed test cycle simulation results

The main results of the proposed cycle simulation are reported and analyzed below.

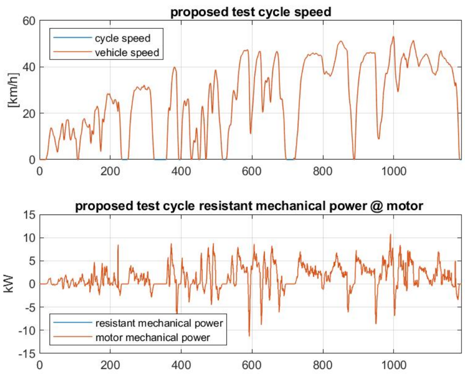

Figure 5.2: Proposed test cycle speed and resistant power @ motor

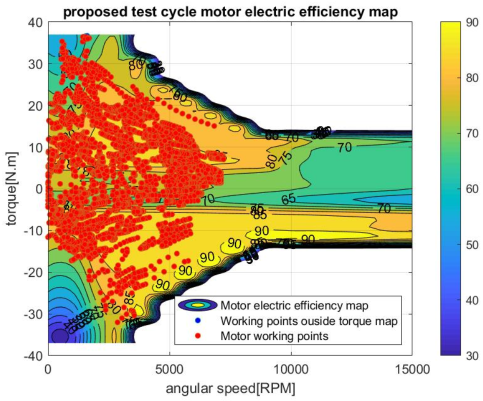

Figure 5.3: Proposed test cycle working points on efficiency map

As can be seen in Figure 5.5 the model can follow in every point the proposed speed profile and the peak value of mechanical power required to the engine is 10.7 kW. Figure 5.3 shows the engine work points and their electrical efficiency, these appear to be distributed over a large region of the map. Comparing them with those of the ECE cycle simulation shown previously in figure 3.4 where instead the points are collected in the regions with higher efficiency, it is evident that the proposed cycle is more suitable than the ECE that was previously used for the homologation of vehicles of category L.
Figures 5.4 compare graphs representing the behavior of the battery and the electrical energy consumption of the vehicle, simulating the cycle in the two initial conditions of SOC = 1(i.e. fully charged battery) and SOC = 0.1 (i.e. almost empty battery).These graphs highlight the inverse dependence of the internal resistance and the direct dependence of the open-circuit voltage of the battery on the SOC already shown while creating the model respectively in figure 2.17 and 2.16.The variation of these parameters due to the discharge of the battery results in an increase in the intensity of the current and consequently in the amount of charge that the battery must supply to the vehicle to satisfy the same electrical energy demand.Said in another way, the dependence of the battery's behavior on the SOC implies that the vehicle will not always discharge the battery by the same percentage of SOC, but this percentage will increase as the SOC decreases. Moreover, it is important to note that the maximum electrical power estimated by the model that the battery can provide is dependent on the $R_{batt_{eq}}$ and the OCV_{batt}

and consequently the SOC.Therefore, the battery may not always be able to provide the power required for the cycle, but this will depend on the SOC.In table 5.2 are collected the main results of the proposed cycle simulation and also three values for ranges of the vehicle: the first two obtained considering the consumption achieved for the initial SOC values simulated and the third more realistic obtained from the average of the two.

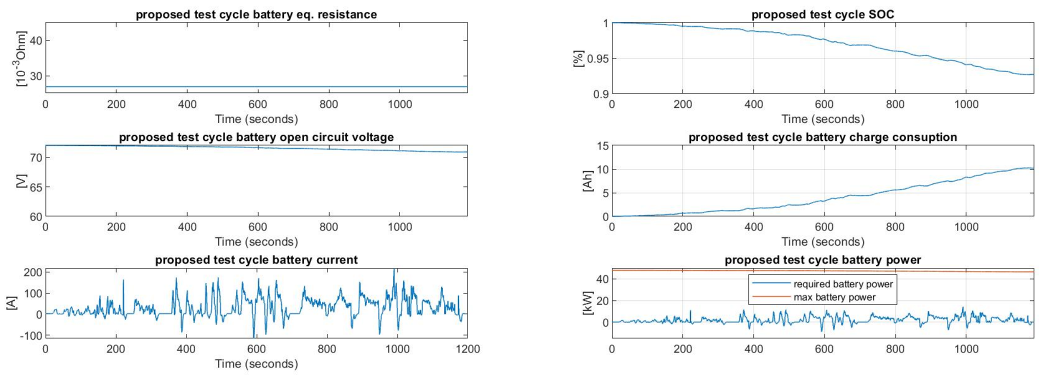

Figure 5.4: Proposed test cycle battery behaviour and charge consumption @ initial SOC=1

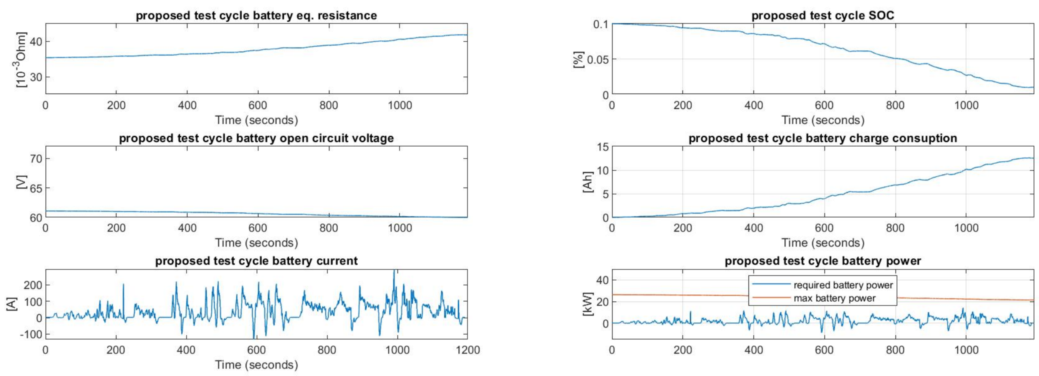

Figure 5.5: Proposed test cycle battery behaviour and charge consumption @ initial SOC=0.1

	proposed cycle characteristics	
energy request $[kJ]$ **no reg .braking**	2002	
energy request $[kJ]$ **100% reg .braking**	1294	
peak power request $[kW]$	10.7	
	Initial condition SOC=1	**Initial condition SOC=0.1**
charge consumption $[Ah]$	10.1	12.6
Δ **SOC** $[\%]$	7.3	9.1
estimated range $[km]$	117	86
mean range $[km]$	101	

Table 5.2: Proposed cycle results

5.2 Test procedure definition

The last step of this work is to try to define guidelines for the energy efficiency test of L7 category electric vehicles. The test must be carried out in a laboratory in standard condition of temperature and pressure ($T = 20° \ C$, $P = 1 \ atm$) using a chassis dynamometer, a device capable of simulating in a controlled environment the resistant forces exerted in road driving.the vehicle must be tested with the battery fully charged and allowing sufficient soaking time in the laboratory to achieve thermal equilibrium.
As shown before, vehicle consumption is SOC-dependent, so to obtain a reliable value, it is not sufficient to complete the driving cycle once, but the test must continue until the battery is completely discharged or until the power supplied by the battery is no longer sufficient for the vehicle to follow the speed profile.This gives a measure of the vehicle's autonomy, and the energy consumed is estimated by recharging the battery through a cable equipped with a current meter.Finally dividing the energy used to recharge the battery (which also takes into account the losses given by the internal resistance of the battery) by the traveled distance during the test it is obtained the energy consumption for kilometer.
Moreover, even if the proposed model does not take into account the effect of temperature on the battery, the performance of electric vehicles is very dependent on environmental conditions so it would be appropriate to do similar tests even in low ($T = -\deg 7$) and high temperatures ($T = \deg 40$) to provide consumers with a percentage of oscillation of the range of the vehicle in these conditions.

Chapter 6

Conclusions

This study attempted to analyze the energy consumption of L7 category BEVs. To this end, data provided by experimental tests have been used to build a kinematic model that, having as input a speed profile to follow, can simulate the performance of the vehicle and its consumption.
Due to the lack of technical details of the electric motor and battery system, maps of scaled-down similar components have been used to complete the model. Despite this, the preliminary results conducted on the ECE and EUDC cycles have proven the capabilities of the model, which in terms of mechanical power are in line with those of the simulated vehicle whose speed limit is 50 km/h.
Besides, the experimental test data were used as a reference to compare the simulated SOC, despite the low resolution of the former, it was possible to adjust the model parameters to obtain results closer to the real ones.
The proposed model manages to capture well the behavior of the electric quadricycle and can, therefore, be used to make a preliminary analysis of vehicle performance and consumption. The results of the model were also used as a basis for the definition of a Energy Efficiency test procedure.
A major limitation of the proposed model is the fact that it neglects thermal conditions at which the vehicle operates. This lack must be solved in future studies in fact temperature has a great influence on battery performance and consequently on the range of the vehicle. Moreover, starting from this model it would be useful to define a system to be implemented on BEV vehicles of the category able not only to estimate energy consumption but also to suggest driving strategies to maximize the efficiency of the vehicle.

Appendix A

Results of experimental cycles

Cycle 2

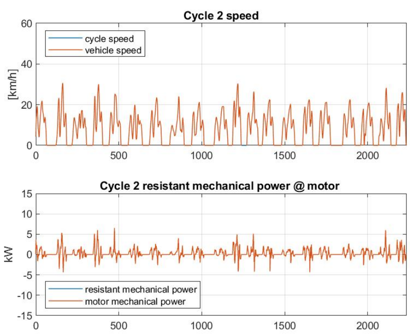

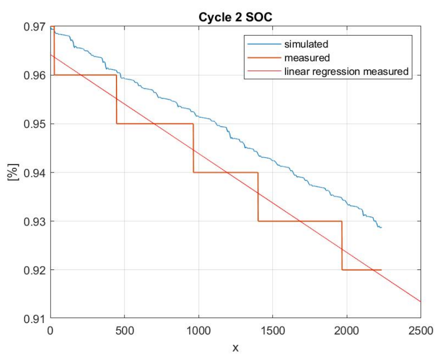

Cycle 3

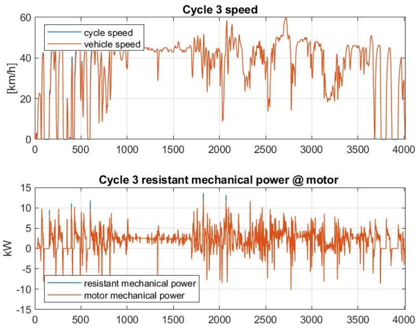

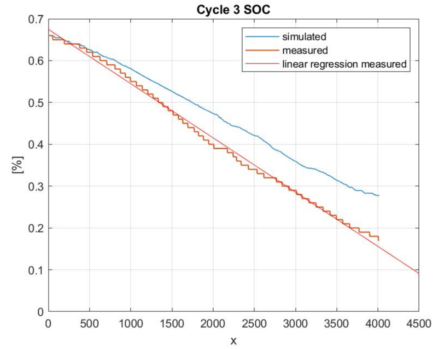

Cycle 5

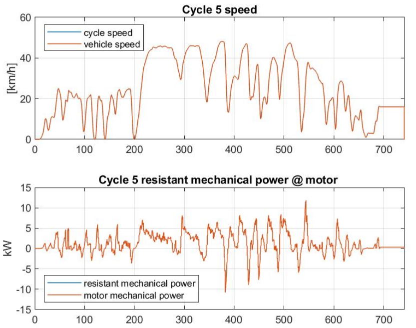

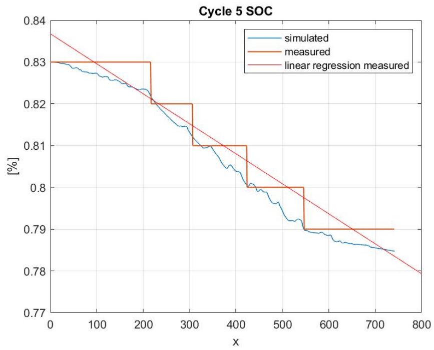

Cycle 6

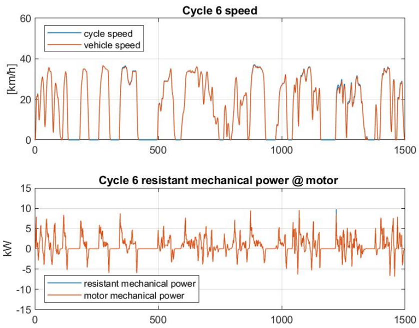

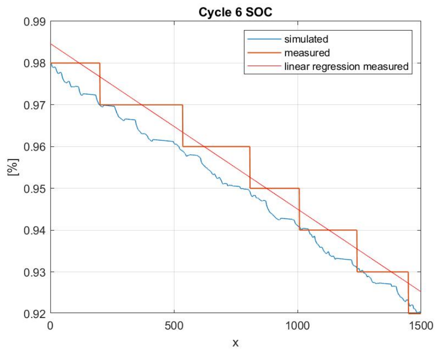

Cycle 7

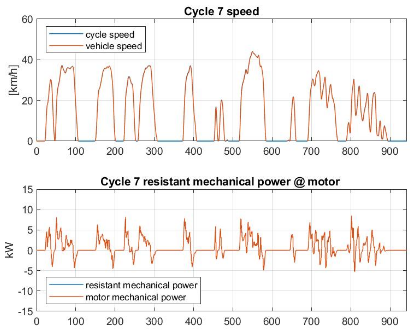

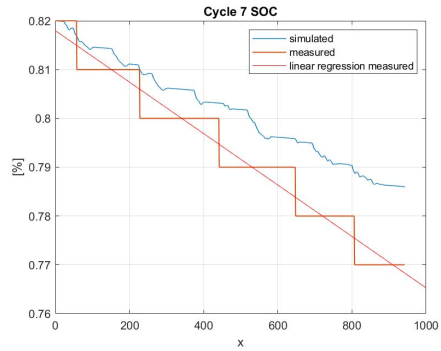

Cycle 8

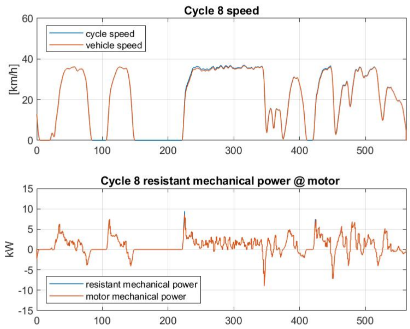

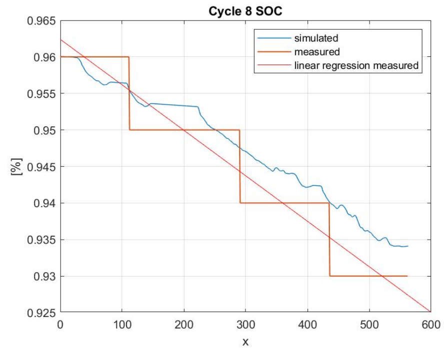

Cycle 9

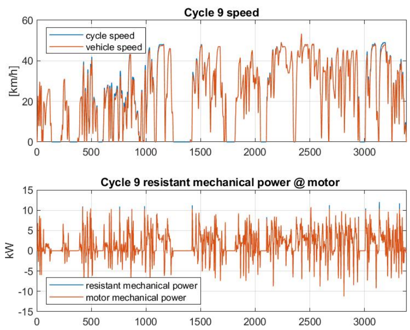

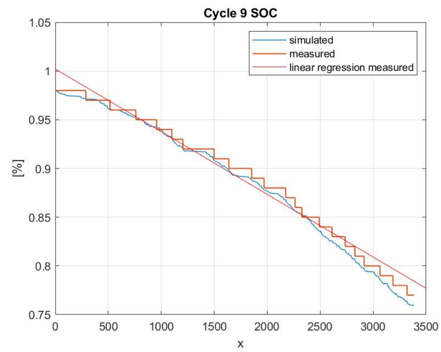

Cycle 10

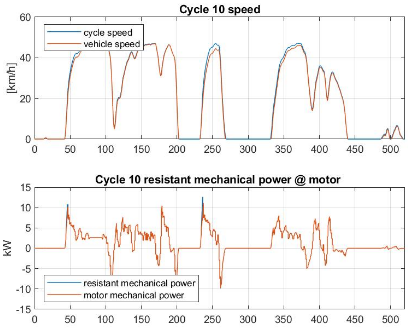

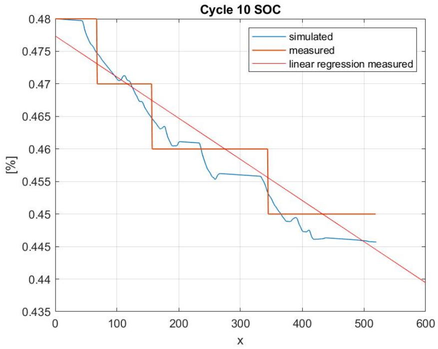

Cycle 11

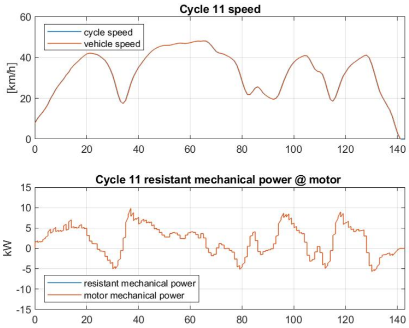

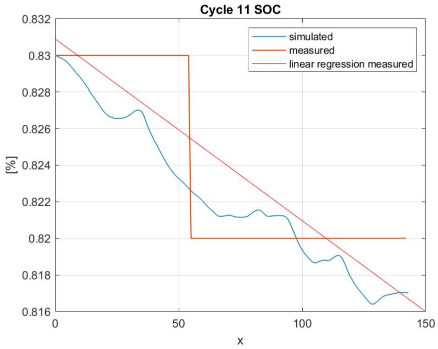

Cycle 12

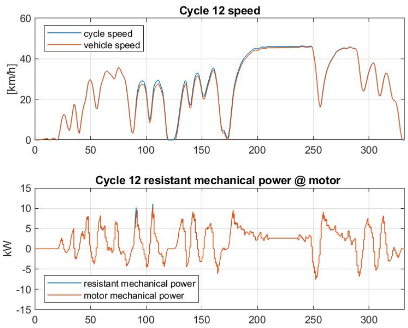

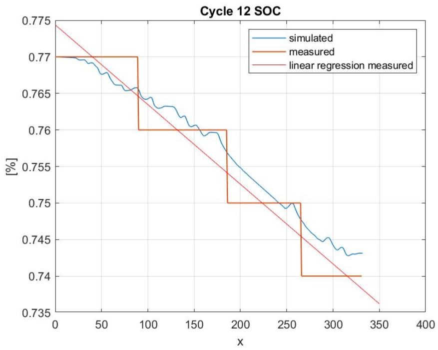

Cycle 13

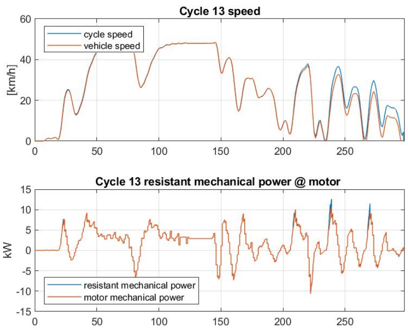

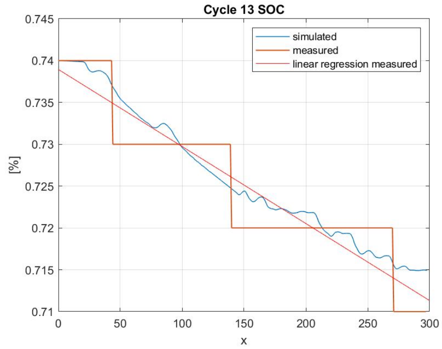

Cycle 14

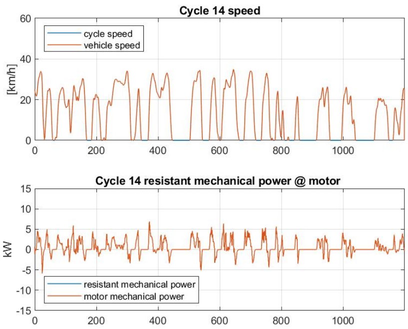

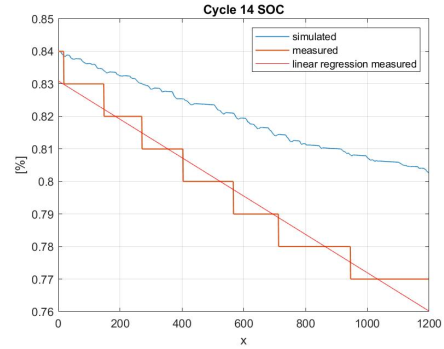

Cycle 15

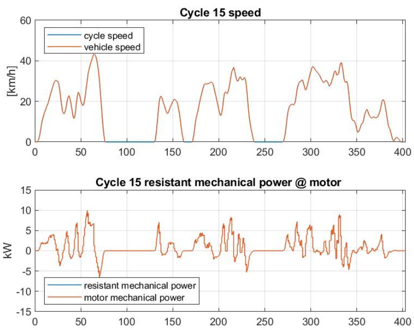

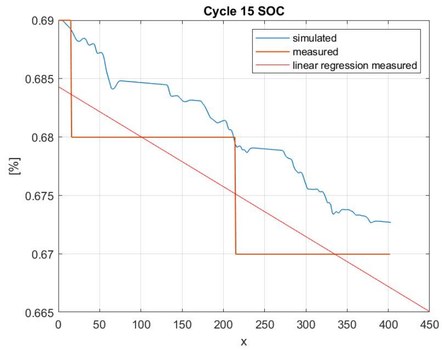

Cycle 16

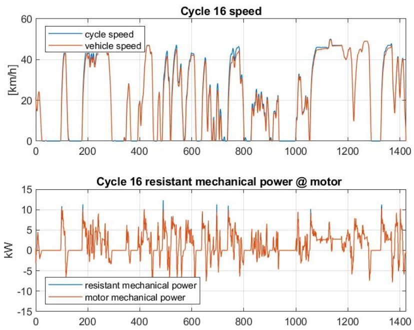

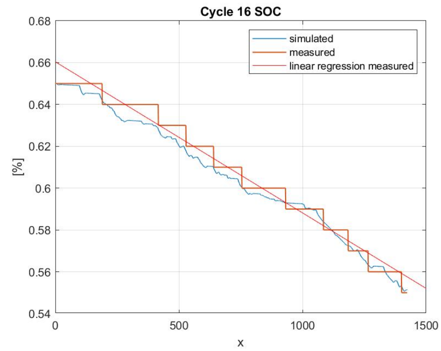

Cycle 17

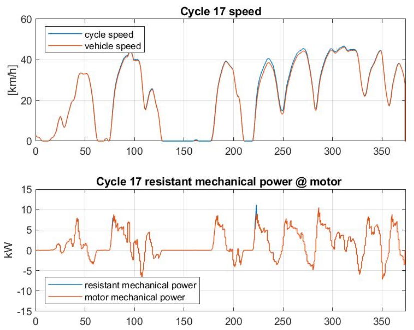

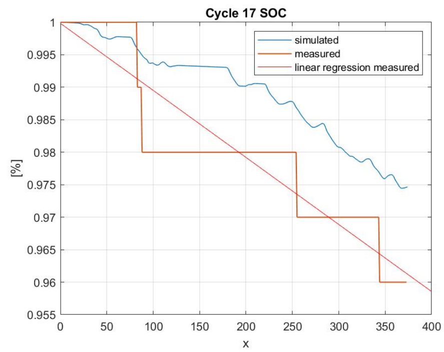

Cycle 18

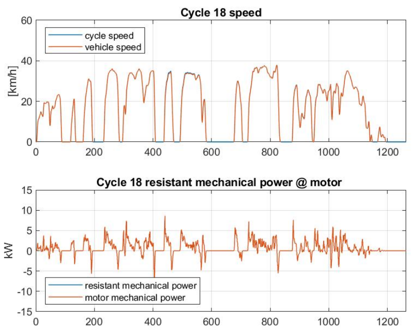

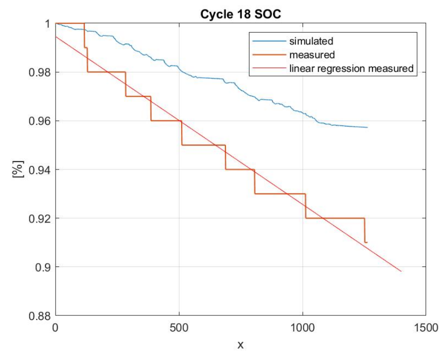

Cycle 20

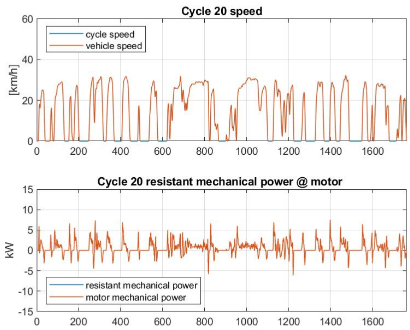

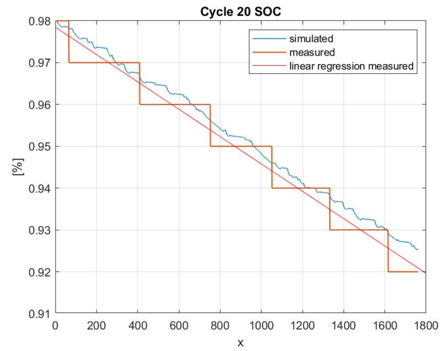

Cycle 21

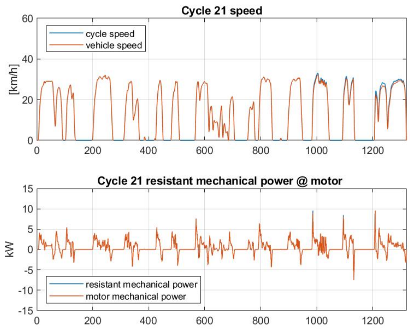

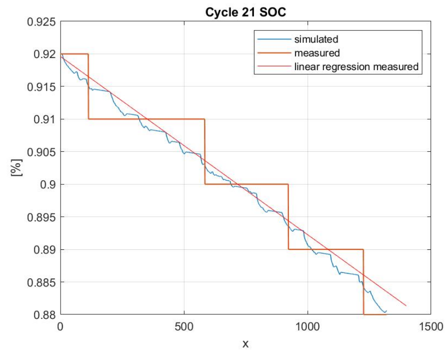

Cycle 22

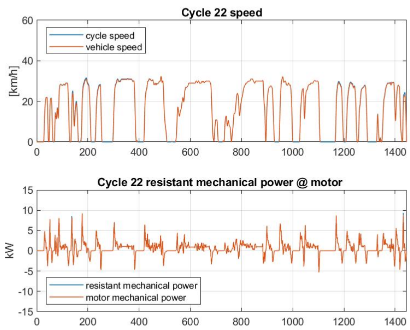

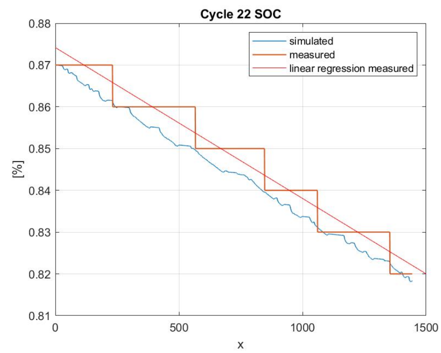

Cycle 23

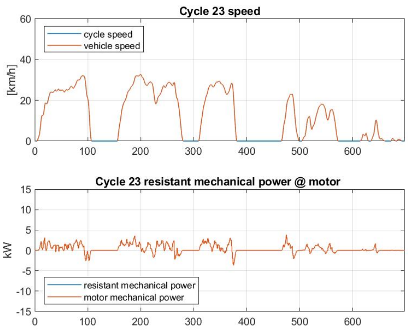

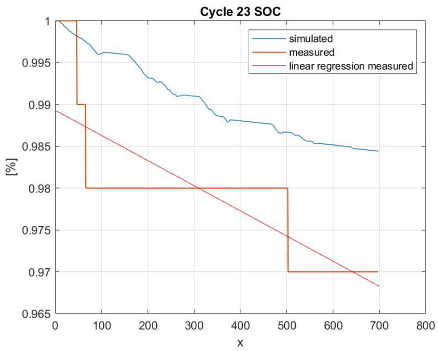

Cycle 24

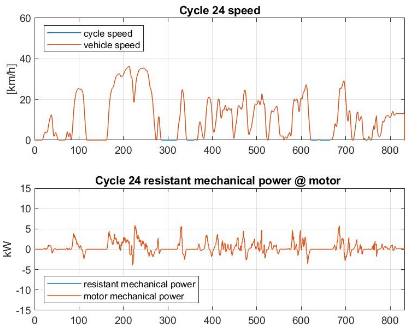

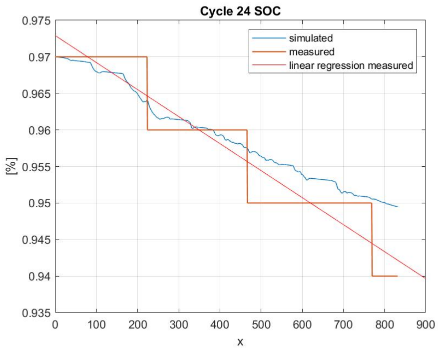

Cycle 25

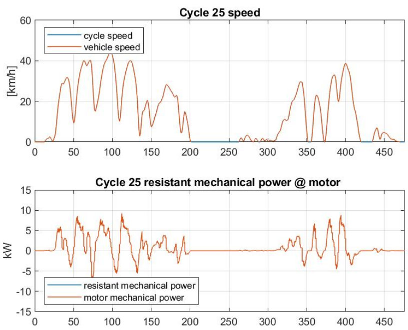

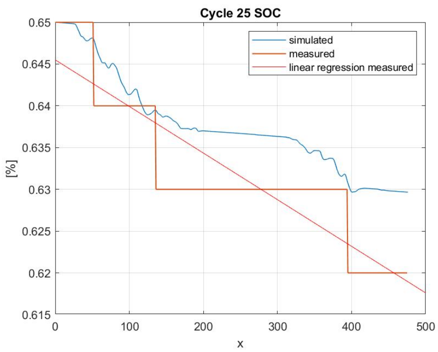

Cycle 26

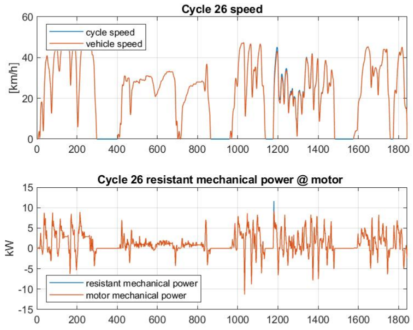

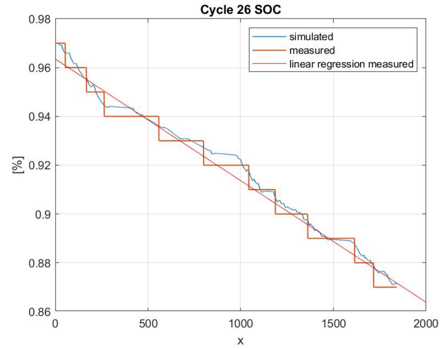

Cycle 27

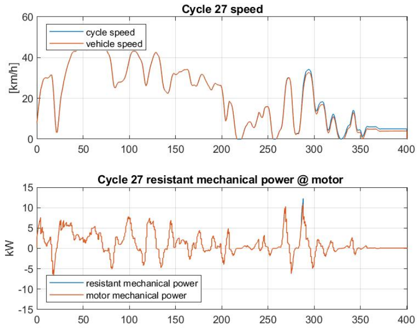

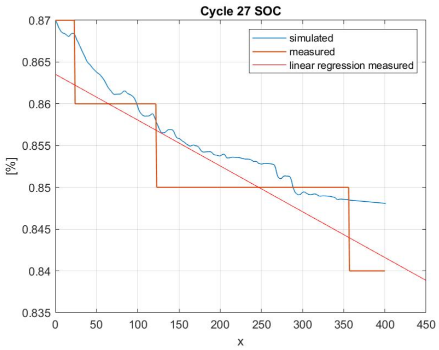

Cycle 28

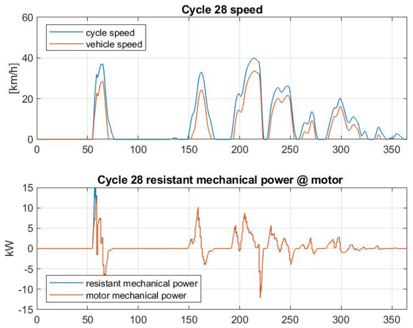

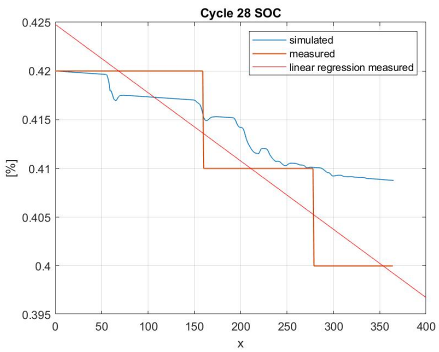

Bibliography

[1] European Parliament and Council of the European Union. *Regulation (EC) No 443/2009 Setting emission performance standards for new passenger cars as part of the Community's integrated approach to reduce CO 2 emissions from light-duty vehicles.* (Text with EEA relevance). 23 April 2009 (cit. on p. 1).

[2] European Parliament and Council of the European Union. *Regulation (EU) 2019/1242 setting CO2 emission performance standards for new heavy-duty vehicles.* and amending Regulations (EC) No 595/2009 and (EU) 2018/956 of the European Parliament and of the Council and Council Directive 96/53/EC. 20 June 2019 (cit. on p. 1).

[3] European Commission. *WHITE PAPER Roadmap to a Single European Transport Area – Towards a competitive and resource efficient transport system.* COM(2011) 144 final. 2011 (cit. on p. 2).

[4] European Parliament and Council of the European Union. *Regulation (EU) No 168/2013 of 15 January 2013 on the approval and market surveillance of two- or three-wheel vehicles and quadricycles.* (Text with EEA relevance). 15 January 2013 (cit. on p. 3).

[5] Danciu G. «Study for an Electrified UTV Platform». In: *Andreescu C., Clenci A. (eds) Proceedings of the European Automotive Congress EAEC-ESFA 2015.* Springer, Cham, 2016, pp. 245–285 (cit. on p. 21).

[6] R. W. Schafer. «What Is a Savitzky-Golay Filter? [Lecture Notes]». In: *IEEE Signal Processing Magazine* 28 (July 2011), pp. 111–117 (cit. on p. 31).